

# IBNorm: Information-Bottleneck Inspired Normalization for Representation Learning

**Xiandong Zou**<sup>1</sup> **Jia Li**<sup>2</sup> **Xiaotong Yuan**<sup>3</sup> **Pan Zhou**<sup>1</sup>

## Abstract

Normalization is fundamental to deep learning, but existing approaches such as BatchNorm, LayerNorm, and RMSNorm are variance-centric by enforcing zero mean and unit variance, stabilizing training without controlling how representations capture task-relevant information. We propose IB-Inspired Normalization (IBNorm), a simple yet powerful family of methods grounded in the Information Bottleneck principle. IBNorm introduces bounded compression operations that encourage embeddings to preserve predictive information while suppressing nuisance variability, yielding more informative representations while retaining the stability and compatibility of standard normalization. Theoretically, we prove that IBNorm achieves a higher IB value and tighter generalization bounds than variance-centric methods. Empirically, IBNorm outperforms BatchNorm, LayerNorm, and RMSNorm across large-scale language models (like LLaMA, GPT-2) and vision models (e.g., ResNet, ViT), with mutual information analysis confirming superior information bottleneck behavior. Code will be released publicly and is available in the supplementary now.

## 1. Introduction

Normalization has become a cornerstone of deep learning, credited for stabilizing and accelerating training across domains. Techniques such as Batch Normalization (BN) (Ioffe & Szegedy, 2015), Layer Normalization (LN) (Ba et al., 2016), and RMSNorm (Zhang & Sennrich, 2019) are now standard in architectures spanning vision and language (Vaswani et al., 2017; Dosovitskiy et al., 2020; He et al., 2016a), underscoring normalization as a key driver of training stability and acceleration.

<sup>1</sup>Singapore Management University <sup>2</sup>Beijing Normal University <sup>3</sup>Nanjing University. Correspondence to: Pan Zhou <panzhou@smu.edu.sg>.

*Preprint. January 30, 2026.*

Despite this success, existing normalization methods share a fundamental limitation: they are inherently *variance-centric*. By enforcing zero mean and unit variance, followed by rescaling and shifting, they improve the conditioning of the optimization problem (Huang et al., 2023; 2018; He et al., 2016b; Desjardins et al., 2015). However, this process operates purely on first- and second-order statistics, without offering any guidance on (intermediate) representation learning. Indeed, two representations may share identical mean and variance, but can encode drastically different amounts of task-relevant information (Raginsky et al., 2016; Achille & Soatto, 2018a). This raises a key question: can normalization be re-designed not only to stabilize training but also to shape representations toward sufficiency and generalization?

Prior works have explored this direction. For instance, NormalNorm (Eftekhar & Popyan, 2025) encourages Gaussian-like features via power transforms and additive noise, arguing that maximizing feature entropy improves representation learning. We argue that this objective is misaligned with generalization: Gaussian-like activations indiscriminately retain task-irrelevant nuisance factors and cannot filter task-irrelevant information (Kawaguchi et al., 2023; Tishby & Zaslavsky, 2015; Saxe et al., 2019). Additionally, NormalNorm destabilizes the zero-mean, unit-variance properties essential for efficient optimization (see Appendix B).

**Contributions.** In this work, we move beyond variance-centric normalization and introduce **IBNorm**, a simple yet powerful normalization method grounded by the Information Bottleneck (IB) principle (Shamir et al., 2010; Tishby & Zaslavsky, 2015; Shwartz-Ziv & Tishby, 2017). Moreover, we also theoretically justify the superiority of IBNorm and its better generalization performance.

First, we introduce an IB perspective to normalization, and propose IBNorm for generalization improvement. The IB principle seeks representations that preserve task-relevant information while discarding nuisances, thereby connecting normalization to generalization. Within this framework, we decompose existing normalization methods into three steps: (i) grouping features (e.g., across batch, channel, or dimension), (ii) standardization, and (iii) recovery via re-scaling and shifting. Our analysis reveals that the normalization operation itself is the key bottleneck governing information

---

flow. Building on this insight, IBNorm introduces several different compression operators that selectively compress activations toward their means, providing explicit control over sufficiency-redundancy tradeoffs while remaining drop-in compatible with existing architectures.

Second, we provide theoretical guarantees. Under the IB framework, we prove that IBNorm achieves a strictly larger IB value than variance-centric methods like LN and BN, thereby better balancing predictive sufficiency with nuisance suppression. Moreover, we establish a provably tighter generalization bound, explaining why IBNorm outperforms standard normalization in practice.

Extensive experiments show the effectiveness of IBNorm across architectures and modalities. In language modeling, integrating IBNorm into LLaMA (Touvron et al., 2023b) and GPT-2 (Radford et al., 2019) outperforms LN, RMSNorm, and NormalNorm on LLM Leaderboard I/II by up to 8.75%. In vision, applying IBNorm to ResNet (He et al., 2016a) and ViT (Dosovitskiy et al., 2020) yields substantial gains, e.g., 3.98% improvement (ResNet-50) and 8.17% improvement (ViT) on ImageNet (Deng et al., 2009).

## 2. Related Work

### 2.1. Normalization

Normalization plays a central role in modern deep learning, enabling faster convergence and improved generalization across natural language processing (NLP) (Vaswani et al., 2017; Touvron et al., 2023a;b; Dubey et al., 2024; Bai et al., 2023; Liu et al., 2024) and computer vision (CV) (He et al., 2016a; Dosovitskiy et al., 2020; Liu et al., 2022).

Batch Normalization (BN) (Ioffe & Szegedy, 2015) normalizes activations across mini-batches to stabilize training, with numerous extensions such as Mean-only BN (Salimans & Kingma, 2016),  $L^p$ -Norm BN (Liao et al., 2016), Conditional BN (De Vries et al., 2017), and Whitening BN (Siarohin et al., 2018; Huang et al., 2018; 2019). Layer Normalization (LN) (Ba et al., 2016) was proposed for sequential and small-batch settings and has inspired variants including Dynamic LN (Kim et al., 2017), RMSNorm (Zhang & Senrich, 2019), and Adaptive LN (Xu et al., 2019), which are now standard in Transformers (Vaswani et al., 2017; Dosovitskiy et al., 2020). Group Normalization (GN) (Wu & He, 2018) and Batch Group Normalization (BGN) (Summers & Dinneen, 2019) extend this idea by combining grouping across features, channels, or batches. Collectively, these methods underscore normalization as a structural tool for scaling depth and stabilizing optimization (Huang et al., 2023; Xu et al., 2019; Joudaki et al., 2023).

Beyond variance-centric approaches, some works attempt to explicitly shape representation distributions. For exam-

ple, Eftekhari & Papyan (2025) encourage Gaussian-like features via power transforms with additive noise, arguing that Gaussianity enhances representational capacity while noise acts as implicit regularization. We identify key theoretical and practical limitations in this approach. The method lacks a principled information-theoretic analysis within the context of deep neural networks. Specifically, the design of NormalNorm is based on the mutual information game (Theorem 2.1 (Eftekhari & Papyan, 2025)) which relies on strong assumptions regarding the first and second moments of the input and noise and neglects higher-order statistics. Consequently, the objective is misaligned with generalization: by prioritizing entropy maximization, the method indiscriminately preserves information, failing to filter task-irrelevant nuisance factors and leading to suboptimal performance. Practically, NormalNorm incurs computational overhead in estimating power parameters and introduces stochasticity that can destabilize training (see Appendix B and C.8).

Broadly, most normalization methods rely on re-centering and rescaling to mitigate internal covariate shift, yet they overlook the information-theoretic properties of representations, such as sufficiency and redundancy. Crucially, even distribution-shaping methods like NormalNorm fail to explicitly balance preserving predictive information against suppressing nuisance factors. These gaps motivates our work. We propose **IBNorm**, which augments conventional normalization with compression operation designed to regulate information flow, guiding activations toward IB-optimal representations that enhance generalization and robustness.

### 2.2. Representation Learning with Explicit Information Bottleneck Objectives

The Information Bottleneck (IB) principle (Tishby et al., 2000; Shamir et al., 2010; Tishby & Zaslavsky, 2015) formulates representation learning as a trade-off between sufficiency and compression. Prior works (Tishby & Zaslavsky, 2015; Alemi et al., 2016; Kolchinsky et al., 2019; Belghazi et al., 2018; Hu et al., 2024) have explored this principle primarily through empirical analysis and leveraging explicit IB objectives during deep learning model training.

Methods such as deep variational information bottleneck (VIB) (Alemi et al., 2016), nonlinear information bottleneck (Kolchinsky et al., 2019), and mutual information neural estimation (MINE) (Belghazi et al., 2018) leverage the IB principle by explicitly estimating mutual information through auxiliary neural MI estimators and incorporating these estimates as IB-regularization terms during training. These approaches rely on encoder-decoder architectures, require large datasets to train accurate MI estimators prior to training the primary model, and introduce additional MI-based loss functions that cause both computational and hyperparameter overhead. The reliance on auxiliary estimators

also imposes architectural constraints and increases the computational burden, a limitation that becomes pronounced in autoregressive LLMs. Furthermore, as demonstrated by MINE, accurate MI estimation requires substantial sample complexity, making these methods expensive and often unstable when applied to large-scale models. Recent techniques such as structured probabilistic coding (Hu et al., 2024) incorporate IB-inspired coding mechanisms but are confined to specific encoder architectures and inherit similar computational and optimization challenges.

Representation learning methods based on explicit IB objectives face many limitations: they impose heavy computational overhead due to auxiliary MI-estimator networks, introduce architectural constraints, and require large sample sizes for accurate mutual information estimation. Detailed discussion can be found in Appendix A.1 and A.2.

To effectively integrate the IB principle into modern deep learning models, IBNorm introduces the first framework to internalize the IB principle directly within the normalization operation. By redesigning the normalization layer to act as an information filter, IBNorm achieves the benefits of IB-guided compression—improved generalization and robustness—without computationally expensive auxiliary estimators, external losses, or architectural constraints.

### 3. Preliminary

Here we introduce information bottleneck (IB) framework (Shamir et al., 2010; Tishby & Zaslavsky, 2015) which forms the basis of our approach in Sec. 4.

Consider two random variables  $X$  and  $Y$  with joint probability densities  $p(x, y)$  over the space  $\mathcal{X} \times \mathcal{Y}$ . We can define the mutual information between  $X$  and  $Y$ :

$$I(X; Y) = \int_{x \in \mathcal{X}} \int_{y \in \mathcal{Y}} p(x, y) \log \frac{p(x, y)}{p(x)p(y)} dx dy. \quad (1)$$

Mutual information measures dependencies between random variables, and can be understood as how much knowing  $X$  reduces the uncertainty in  $Y$  or vice versa (Hjelm et al., 2018; Gabrié et al., 2018; Kong et al., 2019).

Building on this, the IB framework formulates representation learning as a trade-off between two goals: 1) minimality which compresses  $X$  by reducing  $I(X; T)$ ; and 2) sufficiency which preserves information about  $Y$  by maximizing  $I(Y; T)$ . This is captured by the IB objective:

$$\max_T [I(Y; T) - \beta I(X; T)], \quad (2)$$

where  $\beta > 0$  (Tishby & Zaslavsky, 2015). Here,  $T$  must satisfy the Markov chain  $T - X - Y$ , and the optimal representation  $T^*$  is given by the conditional distribution  $p_{T^*|X}(t|x)$  with marginal  $p_{T^*}(t) = \int p_{T^*|X}(t|x)p_X(x)dx$  governed by self-consistency equations (Tishby et al., 2000).

Intuitively, maximizing  $I(Y; T)$  ensures that the representation  $T$  preserving information relevant for predicting the tar-

get  $Y$ , thereby enhancing predictive power and interpretability. Concurrently, penalizing  $I(X; T)$  enforces compression, which eliminates irrelevant variability in the representation and, in turn, enhances generalization and robustness of the representation (Kawaguchi et al., 2023; Goldfeld & Polyaniskiy, 2020; Saxe et al., 2019; Federici et al., 2020).

## 4. Methodology

Inspired by the IB principle introduced in Sec. 3, we present how it motivates an effective normalization strategy — an essential component of modern deep learning architectures.

### 4.1. Normalization Design via IB Principle

**Normalization decomposition and limitations.** Consider a data space  $\mathcal{X}$  and label space  $\mathcal{Y}$  with a fixed joint distribution  $\mathbb{P}(X, Y) \in \mathcal{P}(\mathcal{X} \times \mathcal{Y})$ . A feedforward neural network  $f(\cdot; \theta)$ , parameterized by  $\theta$ , maps an input  $X \in \mathcal{X}$  to a prediction  $\hat{Y} = f(X; \theta)$ , aiming to approximate the ground-truth label  $Y$ . Here,  $f(\cdot; \theta)$  can represent various architectures, such as convolutional neural networks (e.g., ResNet (He et al., 2016a)) and transformer-based networks (e.g., large language models like (Touvron et al., 2023b) or vision transformer (Dosovitskiy et al., 2020)).

For an  $L$ -layer network with normalization, we write the intermediate representation after the  $l$ -th normalization as:

$$T_l := \Phi_l \circ h_l \circ \dots \circ \Phi_1 \circ h_1(X) \in \mathcal{T}_l, \quad l \in \{1, \dots, L\}, \quad (3)$$

where  $\mathcal{T}_l$  is a measurable space,  $h_i$  is a transformation block with parameter  $\theta_i$ , and  $\Phi_i$  is the normalization layer, e.g., layer normalization. We use symbol  $\circ$  to represent the composition of functions. Following (Huang et al., 2023), any normalization layer  $\Phi$  can be decomposed as:

$$\Phi(\cdot) \equiv \eta \circ \psi \circ \zeta, \quad (4)$$

where  $\zeta$  defines the *normalization area partitioning* (NAP), i.e., how features are grouped (e.g., batch-level in BN, feature-level in LN, or group-level in GN);  $\psi$  is the *normalization operation* (NOP), i.e., the standardization operation;  $\eta$  is the *normalization representation recovery* (NRR), typically an affine re-scaling and shifting.

This decomposition unifies existing normalization methods. For instance, BN (Ioffe & Szegedy, 2015), LN (Ba et al., 2016), and GN (Wu & He, 2018) differ mainly in their choice of NAP ( $\zeta$ ): BN normalizes across the batch dimension, LN across the feature dimension, and GN across groups of features. In all cases, the NOP enforces zero-mean and unit-variance statistics, while the NRR rescales and shifts the result. Crucially, among them, NAP ( $\zeta$ ) is often dictated by the network architecture or task domain (e.g., batch-based normalization favored by CNNs, feature-based normalization for Transformers). Likewise, NRR ( $\eta$ ) is linear and invertible, and therefore only re-parameterizes activations without altering their information content. This

leaves the NOP ( $\psi$ ) as the main degree of freedom: it governs how information is filtered and thus determines whether normalization merely stabilizes optimization or also enhances the quality of learned representations.

However, most existing NOP ( $\psi$ ) operations are fundamentally variance-centric, enforcing zero-mean and unit-variance scaling of activations. While stabilizing and accelerating training, it overlooks whether the resulting representations retain task-relevant information. From the IB perspective in Sec. 3, it reveals a fundamental limitation: variance normalization alone cannot guarantee the balance between sufficiency (retaining predictive information) and minimality (removing redundancy). As a result, relying solely on variance-centric NOP ( $\psi$ ) can produce representations with superior generalization and robustness, since higher IB values are empirically and theoretically linked to better generalization and robustness (Kawaguchi et al., 2023; Alemi et al., 2016; Goldfeld & Polyanskiy, 2020; Saxe et al., 2019; Achille & Soatto, 2018b).

**IB-guided normalization objective.** The IB framework provides a principled way to rethink normalization. An ideal intermediate representation  $T_l$  should satisfy two criteria: 1) preserve sufficiency, namely, maximizing the predictive information  $I(Y; T_l)$  about the target and thus representation  $T_l$  can easily predict the target  $Y$ ; and 2) promote compression, i.e., minimizing task-nuisance information  $I(T_{l-1}; T_l)$  carried over from the previous layer and thereby removing the potential unimportant noises or patterns. This intuition leads to the following multi-layer IB objective:

$$\max_{\{T_l\}_{l=1}^L} \sum_{l=1}^L \left( I(Y; T_l) - \beta I(T_{l-1}; T_l) \right), \quad (5)$$

where  $\{T_l\}_{l=1}^L \in \mathcal{T}_1 \times \dots \times \mathcal{T}_L \equiv \mathcal{T}^{\otimes L}$ ,  $T_0 = X$  and  $\beta > 0$  controls the trade-off between sufficiency and compression. Prior works (Kawaguchi et al., 2023; Saxe et al., 2019; Alemi et al., 2016; Goldfeld & Polyanskiy, 2020; Achille & Soatto, 2018b) has shown that both generalization error and robustness positively correlate with the IB value in Eqn. (5), implying that aligning intermediate representations with the IB principle can improve generalization and robustness.

Building on this insight, we aim to enhance conventional variance-centric NOP ( $\psi$ ) operator with an IB-inspired compression operation. Rather than treating normalization as a mere stabilizer, we reinterpret it as an information filter that produces representations that are both compact and predictive, bridging optimization stability and information-theoretic optimality. Directly optimizing Eqn. (5) as an additional IB-based training loss is infeasible due to two main reasons: (1) the computational cost of estimating mutual information using auxiliary MI neural estimators over the unknown joint distribution  $p_{X,Y}$ , and (2) the significant training overhead and sample complexity associated with such MI neural estimators (see details in Appendix A.2).

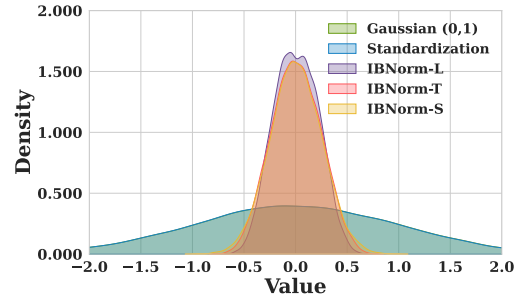


Figure 1. Comparison of kernel density estimation for Gaussian inputs (mean 0, varying variance) under different compression operations: Standardization, IBNorm-L, IBNorm-T, and IBNorm-S ( $\lambda = 4$ ). See more examples in Appendix C.6.

However, it provides a guiding principle: normalization should go beyond variance standardization to encourage information-preserving activations. We introduce our IB-inspired normalization in Sec. 4.2 and theoretically justify its superiority and improved generalization in Sec. 4.3.

## 4.2. IB-Inspired Normalization

In Sec. 4.1, we identified a key limitation of existing normalization methods: their variance-centric design does not guarantee that intermediate representations preserve task-relevant information. Guided by the IB principle, our goal is to design a normalization operator that explicitly reshapes activations into information-preserving forms, rather than merely controlling their variance.

To this end, we propose an IB-inspired normalization. Unlike conventional variance-centric approaches, which manipulate only first- and second-order activation statistics via standardizing activations to have zero mean and unit variance, our approach introduces an extra compression operation into the normalization operation (NOP)  $\psi$  that acts on higher-order statistics. Specifically,  $\psi$  compresses activations toward their mean in a controlled manner, thereby increasing local kurtosis and inducing sparsity in activations across instances. Prior work has shown that mean-centered and sparse representations, where most activations concentrate around the mean, often exhibit stronger generalization by filtering redundant and task-nuisance variability from the tail regions (Olshausen & Field, 1997; Ranzato et al., 2007; Bengio et al., 2013; Zhang et al., 2018; Guo et al., 2019). Motivated by this insight, our compression operation suppresses variability in activation tails, reshaping the higher-order distribution of activations rather than merely rescaling and shifting activations. Importantly, we find this design aligns normalization with the IB principle, preserving target-relevant information  $I(Y; T_l)$  while suppressing irrelevant task-nuisance information  $I(T_{l-1}; T_l)$  (Sec. 4.3).

**Compression operation in IBNorm.** Here we introduce the normalization operation (NOP)  $\psi$  in our IBNorm. Let  $X$  be hidden activations from a given layer, and let  $x =$

$\{x_i\}_{i=1}^H$  represent a sample of  $H$ -dimensional activations. We define the compression operation  $s_\lambda(\cdot; \lambda) : \mathbb{R}^d \rightarrow \mathbb{R}^d$ :

$$s_\lambda(x_i; \lambda) = \mu + \text{sign}(x_i - \mu) \cdot f_\lambda(|x_i - \mu|), \quad (6)$$

where  $\mu = \frac{1}{H} \sum_{i=1}^H x_i$  is the mean activation, and  $f_\lambda(|x_i - \mu|)$  is a measurable and strictly monotone non-decreasing function with a hyper-parameter  $\lambda$  satisfying the *bounded compression property*:

$$0 \leq f_\lambda(r) \leq \alpha_\lambda r, \quad \forall r \geq 0, \quad \alpha_\lambda \in [0, 1]. \quad (7)$$

The property (7) increases local kurtosis and reduces the spread of the distribution in activations by compressing activations toward the mean. This compression suppresses variability in the tail regions, which often encode task-irrelevant fluctuations in the high-dimensional activations (Olshausen & Field, 1997; Hyvärinen & Oja, 2000). As a result, the compression operation decreases task-nuisance information with the input,  $I(T_{l-1}; T_l)$ , while preserving the main mass of the distribution that carries task-relevant information,  $I(Y; T_l)$ . In other words, by promoting mean-centered activations and inducing effective sparsification in IBNorm, compression encourages representations that retain task-relevant information for the downstream task while attenuating task-nuisance information, consistent with the IB principle, which is also empirically validated in Sec. 4.3.

While the bounded compression property (Eq. 7) establishes the fundamental condition for  $f_\lambda$ , the rate of tail decay remains an important degree of freedom in its design (Chen et al., 2025; Ash & Doléans-Dade, 2000). To systematically explore the design space, we instantiate three representative functionals—IBNorm-S, IBNorm-L, and IBNorm-T—that span a spectrum of tail suppression strength. As visualized in Figures 4–6, these variants apply increasingly stronger suppression to the activation tails: IBNorm-S is the mildest, IBNorm-L is intermediate, and IBNorm-T is the most aggressive. These structural differences manifest in the induced entropy of the representation distribution, leading to different empirical performance. See Appendix C.6 for detailed analysis. Their specific formulations are:

$$\begin{aligned} f_\lambda(|x_i - \mu|) &= |x_i - \mu|/\lambda, & (\text{IBNorm-S}) \\ f_\lambda(|x_i - \mu|) &= \ln(1 + |x_i - \mu|/\lambda), & (\text{IBNorm-L}) \\ f_\lambda(|x_i - \mu|) &= \tanh(|x_i - \mu|/\lambda). & (\text{IBNorm-T}) \end{aligned} \quad (8)$$

For these functionals, the compression ratio  $\alpha_\lambda$  in Eqn. (7) becomes  $\alpha_\lambda = 1/\lambda$ , guaranteeing the bounded compression property whenever  $\lambda \geq 1$ . Thus,  $\lambda$  controls the compression strength: larger  $\lambda$  enforces stronger compression toward the mean  $\mu$ , whereas smaller  $\lambda$  lead to broader activations. This mechanism acts as a structural prior to reduce task-nuisance information while preserving task-relevant information.

**IBNorm.** Building on the foundation of LayerNorm, we introduce *IBNorm*, which integrates an explicit compression operation into the normalization pipeline. This design

preserves the well-known benefits of LayerNorm—training stability and acceleration and architectural compatibility—while also incorporating the information-theoretic advantages of the IB principle. Finally, we derive three variants: IBNorm-S, IBNorm-L, and IBNorm-T.

Formally, given an activation input  $\mathbf{x}$ , IBNorm applies the following sequence of operations: first, the NAP operator  $\zeta$  partitions features in the same way as LayerNorm; next, a compression operator  $s_\lambda$  reduces nuisance variability; then, the NOP operator  $\psi$  standardizes activations and induces effective sparsity in representation based on compression;

$$\text{IBNorm}(\mathbf{x}; \lambda) \equiv \eta \circ \psi \circ s_\lambda \circ \zeta. \quad (9)$$

This hybrid procedure, summarized in Algorithm 1 of Appendix A.3, yields a normalization strategy explicitly guided by the IB principle. We highlight that this differs from the function of nonlinear activations (see Appendix A.1). By construction, IBNorm goes beyond variance normalization: it acts as an *information filter*, enhancing sufficiency by retaining predictive information while improving minimality through compression of irrelevant information in the input. In this way, IBNorm bridges the gap between practical optimization benefits and information-theoretic optimality.

### 4.3. Theoretical Justification of IBNorm

Here we first show that IBNorm achieves a larger IB value in Eqn. (5) than standard normalization methods, and then prove its superior generalization performance.

**Information-theoretic superiority of IBNorm.** To analyze normalization, we consider a simplified setting with two one-layer neural networks,  $f_S = \Phi_S \circ h$  and  $f_{IB} = \Phi_{IB} \circ h$ , that share the same feature extractor  $h$  but differ in their normalization layers:  $\Phi_S \equiv \eta \circ \psi \circ \zeta$  in the baseline network  $f_S$  and  $\Phi_{IB} \equiv \eta \circ \psi \circ s_\lambda \circ \zeta$  in the network  $f_{IB}$  with IBNorm.

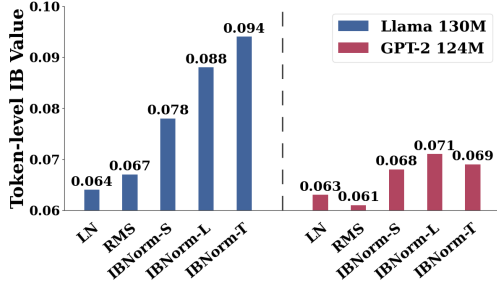
Given the sample dataset  $S = \{x_i, y_i\}_{i=1}^M \sim \mathbb{P}(X, Y)$  containing  $M (< \infty)$  samples, we define the empirical IB value as  $\widehat{IB}_S(T_1) := \widehat{I}_S(Y; T_1) - \beta \widehat{I}_S(X; T_1)$  based on Eqn. (5); therefore, we aim to analyze the empirical IB value of features  $T_S := f_S(X)$  and  $T_{IB} := f_{IB}(X)$ .

Based on the bounded compression property of IBNorm, we can establish the following relationship.

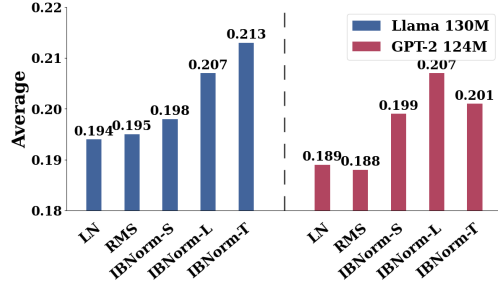
**Theorem 1** (IB Value). *For any hyperparameter  $\beta \in [0, 1]$  and the sample dataset  $S \sim \mathbb{P}(X, Y)$  of size  $M$ , we have*

$$\widehat{IB}_S(T_{IB}) \geq \widehat{IB}_S(T_S) \quad \text{almost surely.} \quad (10)$$

The proof is provided in Appendix E.1. Theorem 1 establishes the theoretical advantage of IBNorm: its compressed features yield higher IB values than those from normalization with standardization, such as LN and BN. Intuitively, IBNorm better preserves label-relevant information  $I(Y; T_{IB})$  while suppressing task-nuisance information



(a) Token-level IB values of Llama-130M and GPT-2 small trained on C4 and OpenWebText, respectively.



(b) Test performance of Llama-130M and GPT-2 small evaluated on the LLM Leaderboard II.

Figure 2. Evaluation of different normalization methods on Llama-130M and GPT-2 small. (a) shows token-level IB values evaluated at the test dataset when training only the normalization layers, and (b) reports test performance on the LLM Leaderboard II.

$I(X; T_{IB})$ , leading to more efficient and predictive representations. Crucially, this benefit holds uniformly across all trade-off parameters  $\beta > 0$ , underscoring the robustness of IBNorm in balancing compression and informativeness.

This result aligns with our empirical results. We train Llama-130M and GPT-2 small with frozen parameters except the normalization layers on C4 (Raffel et al., 2020) and OpenWebText (Gokaslan & Cohen, 2019), respectively. As shown in Fig. 2a, IBNorm consistently achieves higher token-level IB values ( $\beta = 1$ ) compared to variance-centric normalizations, confirming that the compression operation improves information-theoretic optimality. See details in token-level IB value calculation in Appendix G.

**Generalization superiority of IBNorm.** We next extend the analysis to deep multi-layer networks. Motivated by the one-layer result, we expect that IBNorm can increase IB values of multi-layer networks (Appendix C.7), thereby enhancing both expressiveness and compression. To formalize this, we study the generalization gap which measures difference between the expected and empirical-training loss:

$$\text{gen}(S) := \mathbb{E}_{X,Y}[\mathcal{L}(f(X), Y)] - \frac{1}{M} \sum_{i=1}^M \mathcal{L}(f(x_i), y_i), \quad (11)$$

where  $\mathcal{L}$  denotes a per-sample loss. As shown in prior works (Zhang et al., 2016; Neyshabur et al., 2017; Hoffer et al., 2017; Jakubovitz et al., 2019), a smaller  $\text{gen}(S)$  indicates improved generalization performance and robustness theoretically. Without loss of generality, we assume  $\beta = 1$ .

**Corollary 2** (Generalization Bound). *With probability at least  $1 - \delta$  over training set  $S$  of size  $M < \infty$ , the generalization error of a  $L$ -layer network  $f_o$  satisfies*

$$\text{gen}(S; f_o) \leq U_o := \sum_{l=1}^L U_l^o, \quad (12)$$

with  $U_l^o = \sqrt{\frac{-IB(T_l^o) + C_S + \log(\frac{2}{\delta})}{M}}$ ,

where  $T_l^o$  is the intermediate representation at layer  $l$ , and  $C_S$  is a term depending on the cardinality of the training set  $S$ . Here  $f_o$  can be the network  $f_S$  using standard normalization like LN and BN, or the network  $f_{IB}$  with IBNorm.

See Appendix E.4 for the proof. Corollary 2 establishes that the overall generalization gap depends on the quantity  $-IB(T_l^o)$  which measures the amount of task-irrelevant input information preserved in the representations.

By Theorem 1, IBNorm increases the IB value of the population distribution at each layer, thereby reducing  $-IB(T_l^{IB})$  compared to  $-IB(T_l^S)$ . Summing across layers, we obtain  $U_{IB} \leq U_S$ , which shows that the generalization bound of the IBNorm network is tighter than that of the standard network. This implies that  $f_{IB}$  achieves superior generalization performance compared to  $f_S$ . In Fig. 2b, we follow the setting in Fig. 2a to train Llama-130M and GPT-2 small. Evaluation under LLM Leaderboard II shows that IBNorm improves generalization performance, consistent with the information-theoretic (Kawaguchi et al., 2023) and empirical studies (Zhu et al., 2025; Chen et al., 2025).

## 5. Experiment

We evaluate three variants—IBNorm-S, IBNorm-L, and IBNorm-T—across LLM pretraining and vision classification, comparing against LN (Ba et al., 2016), BN (Ioffe & Szegedy, 2015), RMSNorm (Zhang & Sennrich, 2019), and NormalNorm (Eftekhari & Popyan, 2025).

**LLM pretraining.** We pretrain LLaMA series (Touvron et al., 2023b) (60M-1B) on C4 (Raffel et al., 2020), following (Lialin et al., 2023; Zhao et al., 2024), and GPT-2 (124M and 355M) on OpenWebText (Gokaslan & Cohen, 2019), following the Sophia setup (Liu et al., 2023) with the nanoGPT implementation (Karpathy, 2022). See details in Appendix F.1. We report performance on LLM Leaderboards I & II (Beeching et al., 2023; Fourrier et al., 2024).

**Vision training.** We train ResNet-18 on CIFAR-10 (Krizhevsky et al., 2009) and ResNet-50 and ViT on ImageNet (Deng et al., 2009), following the setup (Eftekhari & Popyan, 2025). Both top-1 and top-5 accuracies are reported. Detailed settings are provided in Appendix F.2. Extended results of ViT-S/16 and ViT-B/16 (Dosovitskiy et al., 2020) on ImageNet can be found in Appendix C.5.

Table 1. Results of Llama models evaluated on LLM Leaderboard II and I. Due to space limitation, we defer the results of each task on Leaderboard I to Tab. 6 of Appendix C.1.

Model	Normalization	Leaderboard II						Leaderboard I AVG (↑)
		IFEval (↑)	BBH (↑)	MATH (↑)	GPQA (↑)	MUSR (↑)	MMLU-PRO (↑)	
Llama 60M	LayerNorm	0.1479	0.2970	0.0000	0.2576	0.3426	0.1071	0.1920
	RMSNorm	0.1274	0.2951	0.0000	0.2634	0.3585	0.1117	0.1924
	NormalNorm	0.1101	0.2876	0.0000	0.2676	0.3571	0.1166	0.1898
	IBNorm-S	0.1915	0.2732	0.0000	0.2534	0.3651	0.1152	0.1997
	IBNorm-L	0.1899	0.3001	0.0000	0.2772	0.3519	0.1137	<b>0.2055</b>
	IBNorm-T	0.1754	0.3013	0.0008	0.2668	0.3598	0.1110	0.2025
Llama 130M	LayerNorm	0.1507	0.2949	0.0000	0.2650	0.3417	0.1116	0.1940
	RMSNorm	0.1274	0.3052	0.0008	0.2643	0.3572	0.1121	0.1945
	NormalNorm	0.1385	0.2888	0.0000	0.2584	0.3611	0.1098	0.1928
	IBNorm-S	0.1343	0.3114	0.0008	0.2601	0.3690	0.1151	0.1984
	IBNorm-L	0.1836	0.3028	0.0000	0.2816	0.3638	0.1124	0.2074
	IBNorm-T	0.1999	0.3053	0.0000	0.2777	0.3783	0.1165	<b>0.2130</b>
Llama 350M	LayerNorm	0.1668	0.2927	0.0000	0.2659	0.3586	0.1178	0.2003
	RMSNorm	0.1673	0.2999	0.0030	0.2667	0.3571	0.1121	0.2010
	NormalNorm	0.1667	0.2940	0.0008	0.2458	0.3599	0.1103	0.1962
	IBNorm-S	0.1447	0.3020	0.0030	0.2940	0.3585	0.1094	0.2019
	IBNorm-L	0.1872	0.3135	0.0000	0.2968	0.3558	0.1162	0.2116
	IBNorm-T	0.1797	0.3115	0.0008	0.2983	0.3788	0.1150	<b>0.2140</b>
Llama 1B	LayerNorm	0.1701	0.3024	0.0038	0.2691	0.3683	0.1183	0.2053
	RMSNorm	0.1693	0.3005	0.0008	0.2685	0.3585	0.1139	0.2019
	NormalNorm	0.1679	0.2971	0.0030	0.2576	0.3656	0.1127	0.2006
	IBNorm-S	0.1572	0.3118	0.0030	0.2958	0.3597	0.1130	0.2067
	IBNorm-L	0.1875	0.3167	0.0038	0.2986	0.3717	0.1171	0.2159
	IBNorm-T	0.1829	0.3155	0.0030	0.2994	0.3793	0.1169	<b>0.2162</b>
								<b>0.3199</b>

Table 2. Results of GPT-2 models evaluated on LLM Leaderboard II and I. Due to space limitation, we defer the results of each task on Leaderboard I to Tab. 7 of Appendix C.1.

Model	Normalization	Leaderboard II						Leaderboard I AVG (↑)
		IFEval (↑)	BBH (↑)	MATH (↑)	GPQA (↑)	MUSR (↑)	MMLU-PRO (↑)	
GPT-2 124M	LayerNorm	0.1010	0.2809	0.0000	0.2718	0.3624	0.1158	0.1886
	RMSNorm	0.0966	0.2772	0.0008	0.2651	0.3730	0.1154	0.1880
	NormalNorm	0.1499	0.2913	0.0000	0.2693	0.3690	0.1119	0.1986
	IBNorm-S	0.1860	0.2793	0.0000	0.2619	0.3540	0.1149	0.1994
	IBNorm-L	0.2207	0.2850	0.0000	0.2650	0.3558	0.1134	<b>0.2067</b>
	IBNorm-T	0.1836	0.2810	0.0000	0.2697	0.3571	0.1158	0.2012
GPT-2 355M	LayerNorm	0.1128	0.2835	0.0000	0.2799	0.3661	0.1106	0.1922
	RMSNorm	0.1395	0.2796	0.0000	0.2694	0.3707	0.1090	0.1947
	NormalNorm	0.1425	0.2899	0.0000	0.2702	0.3708	0.1187	0.1987
	IBNorm-S	0.2069	0.2802	0.0000	0.2716	0.3692	0.1176	0.2076
	IBNorm-L	0.2258	0.2867	0.0000	0.2771	0.3687	0.1163	<b>0.2124</b>
	IBNorm-T	0.1964	0.2824	0.0008	0.2780	0.3719	0.1183	0.2080
								<b>0.3035</b>

## 5.1. Main Results

**Results on LLM.** Due to the space limitation, we defer the results of each task in Leaderboard I to Appendix C.1 and report results with statistical significance in Appendix C.2.

As shown in Tab. 1, IBNorm outperforms variance-centric normalization methods such as LN and RMSNorm. On LLaMA-60M, IBNorm-L achieves average scores of 0.2955 (Leaderboard I) and 0.2055 (Leaderboard II), improving over LN by 1.47% and 7.03%, and over RMSNorm by 2.11% and 6.81%. On LLaMA-350M, IBNorm-T reaches 0.3101 (Leaderboard I) and 0.2140 (Leaderboard II), *i.e.* 1.27% and 6.84% over LN, and 2.51% and 6.46% over RMSNorm. On LLaMA-1B, IBNorm-T achieves the highest scores: 0.3199 on Leaderboard I and 0.2162 on Leader-

board II. Similarly, Tab. 2 also shows that on GPT-2 (355M), IBNorm-L attains 0.3035 (Leaderboard I) and 0.2124 (Leaderboard II), yielding improvements of 2.88% and 9.95% over RMSNorm.

These results demonstrate that IBNorm enhances representation quality in large language models, yielding more predictive and generalizable representations. Further analysis of mutual information and token-level IB values in Appendix C.7 confirms that IBNorm promotes representations that retain task-relevant information while suppressing nuisances, explaining the observed empirical gains. However, IBNorm shows some failure cases (see Appendix C.1).

**Results for vision classification.** Tab. 3 shows that IBNorm also improves performance across vision models and database-

Table 3. Accuracy (%) on image classification tasks. We report BatchNorm’s results for CNNs (ResNet18/50) since it outperforms LayerNorm on CNNs, and present LayerNorm’s results on Transformers (ViT) because it performs much better than BatchNorm.

Normalization	ResNet18 on CIFAR-10		ResNet50 on ImageNet		ViT on ImageNet	
	Top-1	Top-5	Top-1	Top-5	Top-1	Top-5
BatchNorm	93.65	99.85	76.15	92.86	—	—
LayerNorm	—	—	—	—	71.54	89.40
RMSNorm	—	—	—	—	71.03	89.15
NormalNorm	94.01	99.86	77.29	94.04	75.25	<b>92.23</b>
IBNorm-S	95.49	99.85	78.85	94.03	75.82	91.97
IBNorm-L	<b>95.57</b>	<b>99.87</b>	<b>79.18</b>	<b>94.82</b>	<b>76.83</b>	92.22
IBNorm-T	95.51	99.83	78.61	93.79	76.46	92.19

Table 4. Ablation study of Llama 60M with normalization using different  $\lambda$  evaluated on LLM Leaderboard I and LLM Leaderboard II. We defer the detailed results of each task to Appendix C.4.

Normalization	$\lambda$	Leaderboard I		Leaderboard II	
		AVG ( $\uparrow$ )			
IBNorm-S	0.5	0.2898	—	0.1977	—
	4	<b>0.2952</b>	—	<b>0.1987</b>	—
	8	0.2918	—	0.1981	—
IBNorm-L	0.5	0.2863	—	0.2018	—
	4	<b>0.2955</b>	—	<b>0.2055</b>	—
	8	0.2921	—	0.1881	—
IBNorm-T	0.5	0.2881	—	0.1984	—
	4	<b>0.2937</b>	—	<b>0.2025</b>	—
	8	0.2898	—	0.2005	—

Table 5. Ablation study of Llama 60M evaluated on LLM Leaderboard I and LLM Leaderboard II. Due to space limitation, we defer the detailed results of each task to Appendix C.3.

Normalization		Leaderboard I		Leaderboard II	
		AVG ( $\uparrow$ )			
IBNorm-S*		0.2952	—	0.1978	—
IBNorm-S**		0.2881	—	0.1945	—
IBNorm-T*		0.2936	—	0.1956	—
IBNorm-T**		0.2831	—	0.1940	—
IBNorm-L*		0.2905	—	0.1967	—
IBNorm-L**		0.2859	—	0.1934	—

ts. On CIFAR-10, ResNet18 with IBNorm-L achieves 95.57% top-1 accuracy, surpassing BN and NormalNorm by 1.92% and 1.56%. On ImageNet, ResNet50 with IBNorm-L improves over BN and NormalNorm by 3.03% and 1.89%. For ViT, IBNorm-L yields top-1 accuracy gains of 5.29%, 5.80%, and 1.58% over LN, RMSNorm, and NormalNorm.

## 5.2. Ablation Study

**Effects of compression hyper-parameter  $\lambda$ .** We analyze the effect of the hyperparameter  $\lambda$  in our proposed IBNorm, which controls the strength of the compression on intermediate activations. We consider  $\lambda = 0.5, 4, 8$ , corresponding to mild, moderate, and strong compression, respectively. As shown in Tab. 4, the results show that moderate compression ( $\lambda = 4$ ) achieves the best performance, striking a balance between preserving task-relevant information and suppressing irrelevant variability. For instance, IBNorm-S achieves the best scores of 0.2952 and 0.1987. We find that overly mild

and strong compression lead to suboptimal performance, excessively reducing the representation diversity.

**Effects of compression operation and linear affine reparameterization.** To further clarify the design choices underlying our proposed IBNorm, we perform ablation studies on two key components: the compression operation and the standardization step. As reported in Tab. 5, the variant of IBNorm marked with an asterisk (\*) applies standardization before the compression operation, namely,  $\text{IBNorm}(\mathbf{x}; \lambda) \equiv \eta \circ s_\lambda \circ \psi \circ \zeta$ . This modification leads to only minor fluctuations in performance compared to the baseline: for example, the baseline achieves average scores of 0.2950 and 0.1997, while IBNorm-S\* obtains 0.2952 and 0.1978 on Leaderboard I and II, respectively. These results indicate that applying compression operation prior to standardization is preferable for optimal performance. In addition, the variant denoted by a double asterisk (\*\*) removes the linear affine component, which results in a substantial performance drop across benchmarks. For instance, IBNorm-L achieves 0.2955 and 0.2055, whereas IBNorm-L\*\* drops to 0.2859 and 0.1934 on Leaderboard I and II. This pronounced degradation highlights the critical role of the affine reparameterization ( $\eta$ ) in the IBNorm design.

## 6. Conclusion

We revisited normalization through the lens of IB principle and proposed a principled framework for designing normalization layers. We introduced **IBNorm**, a family of non-linear transforms that compress activations toward their mean, yielding more information-rich representations. Without relying on explicit IB objectives during training, IBNorm remains model-agnostic and incurs no heavy computational overhead. Theoretically, we showed that IBNorm achieves stronger information-theoretic optimality—attaining higher IB values and tighter generalization bounds—than variance-centric methods. Empirically, IBNorm outperforms BN, LN, and RMSNorm across vision and language domains.

**Limitations.** Our experiments are limited to medium-scale LLMs due to computational constraints. Extending the evaluation to larger foundation models will be addressed when sufficient computational resources are available.

---

## Impact Statement

The pretrained LLMs employed in this research may reflect biases or generate sensitive or potentially offensive content, intended solely for academic and scientific purposes. The opinions expressed within generated outputs do not represent the views of the authors. We remain committed to fostering the development of AI technologies which align with ethical standards and reflect societal values.

## References

Achille, A. and Soatto, S. Information dropout: Learning optimal representations through noisy computation. *IEEE transactions on pattern analysis and machine intelligence*, 40(12):2897–2905, 2018a.

Achille, A. and Soatto, S. Emergence of invariance and disentanglement in deep representations. *Journal of Machine Learning Research*, 19:1–34, 2018b.

Alemi, A. A., Fischer, I., Dillon, J. V., and Murphy, K. Deep variational information bottleneck. *arXiv preprint arXiv:1612.00410*, 2016.

Ash, R. B. and Doléans-Dade, C. A. *Probability and measure theory*. Academic press, 2000.

Ba, J. L., Kiros, J. R., and Hinton, G. E. Layer normalization. *arXiv preprint arXiv:1607.06450*, 2016.

Bai, J., Bai, S., Chu, Y., Cui, Z., Dang, K., Deng, X., Fan, Y., Ge, W., Han, Y., Huang, F., et al. Qwen technical report. *arXiv preprint arXiv:2309.16609*, 2023.

Beeching, E., Fourrier, C., Habib, N., Han, S., Lambert, N., Rajani, N., Sanseviero, O., Tunstall, L., and Wolf, T. Open llm leaderboard. [https://huggingface.co/spaces/open\\_llm-leaderboard-old/open\\_llm\\_leaderboard](https://huggingface.co/spaces/open_llm-leaderboard-old/open_llm_leaderboard), 2023.

Belghazi, M. I., Baratin, A., Rajeshwar, S., Ozair, S., Bengio, Y., Courville, A., and Hjelm, D. Mutual information neural estimation. In *International conference on machine learning*, pp. 531–540. PMLR, 2018.

Bengio, Y., Courville, A., and Vincent, P. Representation learning: A review and new perspectives. *IEEE transactions on pattern analysis and machine intelligence*, 35:1798–1828, 2013.

Chang, R., Deng, C., and Chen, H. The generalization ridge: Information flow in natural language generation. *arXiv preprint arXiv:2507.05387*, 2025.

Chen, M., Lu, T., Zhu, J., Sun, M., and Liu, Z. Stronger normalization-free transformers. *arXiv preprint arXiv:2512.10938*, 2025.

De Vries, H., Strub, F., Mary, J., Larochelle, H., Pietquin, O., and Courville, A. C. Modulating early visual processing by language. *Advances in neural information processing systems*, 30, 2017.

Deng, J., Dong, W., Socher, R., Li, L.-J., Li, K., and Fei-Fei, L. Imagenet: A large-scale hierarchical image database. In *2009 IEEE conference on computer vision and pattern recognition*, pp. 248–255. Ieee, 2009.

Desjardins, G., Simonyan, K., Pascanu, R., et al. Natural neural networks. *Advances in neural information processing systems*, 28, 2015.

Dosovitskiy, A., Beyer, L., Kolesnikov, A., Weissenborn, D., Zhai, X., Unterthiner, T., Dehghani, M., Minderer, M., Heigold, G., Gelly, S., et al. An image is worth 16x16 words: Transformers for image recognition at scale. *arXiv preprint arXiv:2010.11929*, 2020.

Dubey, A., Jauhri, A., Pandey, A., Kadian, A., Al-Dahle, A., Letman, A., Mathur, A., Schelten, A., Yang, A., Fan, A., et al. The llama 3 herd of models. *arXiv e-prints*, pp. arXiv–2407, 2024.

Eftekhari, D. and Papyan, V. On the importance of gaussianizing representations. *arXiv preprint arXiv:2505.00685*, 2025.

Federici, M., Dutta, A., Forré, P., Kushman, N., and Akata, Z. Learning robust representations via multi-view information bottleneck. *arXiv preprint arXiv:2002.07017*, 2020.

Fourrier, C., Habib, N., Lozovskaya, A., Szafer, K., and Wolf, T. Open llm leaderboard v2. [https://huggingface.co/spaces/open\\_llm-leaderboard/open\\_llm\\_leaderboard](https://huggingface.co/spaces/open_llm-leaderboard/open_llm_leaderboard), 2024.

Gabrié, M., Manoel, A., Luneau, C., Macris, N., Krzakala, F., Zdeborová, L., et al. Entropy and mutual information in models of deep neural networks. *Advances in neural information processing systems*, 31, 2018.

Giraldo, L. G. S., Rao, M., and Principe, J. C. Measures of entropy from data using infinitely divisible kernels. *IEEE Transactions on Information Theory*, 61:535–548, 2014.

Gokaslan, A. and Cohen, V. Openwebtext corpus. *Skylion007*, 2019. URL <http://skylion007.github.io/OpenWebTextCorpus>.

Goldfeld, Z. and Polyanskiy, Y. The information bottleneck problem and its applications in machine learning. *IEEE Journal on Selected Areas in Information Theory*, 1:19–38, 2020.

---

Guo, W., Wang, J., and Wang, S. Deep multimodal representation learning: A survey. *Ieee Access*, 7:63373–63394, 2019.

He, K., Zhang, X., Ren, S., and Sun, J. Identity mappings in deep residual networks. In *European conference on computer vision*, pp. 630–645. Springer, 2016a.

He, K., Zhang, X., Ren, S., and Sun, J. Deep residual learning for image recognition. In *Proceedings of the IEEE conference on computer vision and pattern recognition*, pp. 770–778, 2016b.

Hjelm, R. D., Fedorov, A., Lavoie-Marchildon, S., Grewal, K., Bachman, P., Trischler, A., and Bengio, Y. Learning deep representations by mutual information estimation and maximization. *arXiv preprint arXiv:1808.06670*, 2018.

Hoffer, E., Hubara, I., and Soudry, D. Train longer, generalize better: closing the generalization gap in large batch training of neural networks. *Advances in neural information processing systems*, 30, 2017.

Hu, D., Wei, L., Liu, Y., Zhou, W., and Hu, S. Structured probabilistic coding. In *Proceedings of the AAAI Conference on Artificial Intelligence*, volume 38, pp. 12491–12501, 2024.

Hu, D., Wei, L., Zhou, W., and Hu, S. Impartial multi-task representation learning via variance-invariant probabilistic decoding. In *Proceedings of the 63rd Annual Meeting of the Association for Computational Linguistics (Volume 1: Long Papers)*, pp. 19883–19897, 2025.

Hua, T., Wang, W., Xue, Z., Ren, S., Wang, Y., and Zhao, H. On feature decorrelation in self-supervised learning. In *Proceedings of the IEEE/CVF international conference on computer vision*, pp. 9598–9608, 2021.

Huang, L., Yang, D., Lang, B., and Deng, J. Decorrelated batch normalization. In *Proceedings of the IEEE Conference on Computer Vision and Pattern Recognition*, pp. 791–800, 2018.

Huang, L., Zhou, Y., Zhu, F., Liu, L., and Shao, L. Iterative normalization: Beyond standardization towards efficient whitening. In *Proceedings of the IEEE/CVF conference on computer vision and pattern recognition*, pp. 4874–4883, 2019.

Huang, L., Qin, J., Zhou, Y., Zhu, F., Liu, L., and Shao, L. Normalization techniques in training dnns: Methodology, analysis and application. *IEEE transactions on pattern analysis and machine intelligence*, 45:10173–10196, 2023.

Hyvärinen, A. and Oja, E. Independent component analysis: algorithms and applications. *Neural networks*, 13:411–430, 2000.

Ioffe, S. and Szegedy, C. Batch normalization: Accelerating deep network training by reducing internal covariate shift. In *International conference on machine learning*, pp. 448–456. pmlr, 2015.

Jakubovitz, D., Giryes, R., and Rodrigues, M. R. Generalization error in deep learning. In *Compressed sensing and its applications: third international MATHEOn conference 2017*, pp. 153–193. Springer, 2019.

Joudaki, A., Daneshmand, H., and Bach, F. On the impact of activation and normalization in obtaining isometric embeddings at initialization. *Advances in Neural Information Processing Systems*, 36:39855–39875, 2023.

Karpathy, A. nanogpt. *GitHub repository*, 2022. URL <https://github.com/karpathy/nanoGPT>.

Kawaguchi, K., Deng, Z., Ji, X., and Huang, J. How does information bottleneck help deep learning? In *International conference on machine learning*, pp. 16049–16096. PMLR, 2023.

Kim, T., Song, I., and Bengio, Y. Dynamic layer normalization for adaptive neural acoustic modeling in speech recognition. *arXiv preprint arXiv:1707.06065*, 2017.

Kinga, D., Adam, J. B., et al. A method for stochastic optimization. In *International conference on learning representations (ICLR)*, volume 5. California;, 2015.

Kolchinsky, A., Tracey, B. D., and Wolpert, D. H. Nonlinear information bottleneck. *Entropy*, 21:1181, 2019.

Kong, L., d’Autume, C. d. M., Ling, W., Yu, L., Dai, Z., and Yogatama, D. A mutual information maximization perspective of language representation learning. *arXiv preprint arXiv:1910.08350*, 2019.

Krizhevsky, A., Hinton, G., et al. Learning multiple layers of features from tiny images, 2009.

Lialin, V., Shivagunde, N., Muckatira, S., and Rumshisky, A. Relora: High-rank training through low-rank updates, 2023. URL <https://arxiv.org/abs/2307.05695>.

Liao, Q., Kawaguchi, K., and Poggio, T. Streaming normalization: Towards simpler and more biologically-plausible normalizations for online and recurrent learning. *arXiv preprint arXiv:1610.06160*, 2016.

Liu, A., Feng, B., Xue, B., Wang, B., Wu, B., Lu, C., Zhao, C., Deng, C., Zhang, C., Ruan, C., et al. Deepseek-v3 technical report. *arXiv preprint arXiv:2412.19437*, 2024.

Liu, H., Li, Z., Hall, D., Liang, P., and Ma, T. Sophia: A scalable stochastic second-order optimizer for language model pre-training. *arXiv preprint arXiv:2305.14342*, 2023.

Liu, Z., Mao, H., Wu, C.-Y., Feichtenhofer, C., Darrell, T., and Xie, S. A convnet for the 2020s. In *Proceedings of the IEEE/CVF conference on computer vision and pattern recognition*, pp. 11976–11986, 2022.

Loshchilov, I. and Hutter, F. Decoupled weight decay regularization. *arXiv preprint arXiv:1711.05101*, 2017.

Neyshabur, B., Bhojanapalli, S., McAllester, D., and Srebro, N. Exploring generalization in deep learning. *Advances in neural information processing systems*, 30, 2017.

Olshausen, B. A. and Field, D. J. Sparse coding with an overcomplete basis set: A strategy employed by v1? *Vision research*, 37:3311–3325, 1997.

Radford, A., Wu, J., Child, R., Luan, D., Amodei, D., Sutskever, I., et al. Language models are unsupervised multitask learners. *OpenAI blog*, 1:9, 2019.

Raffel, C., Shazeer, N., Roberts, A., Lee, K., Narang, S., Matena, M., Zhou, Y., Li, W., and Liu, P. J. Exploring the limits of transfer learning with a unified text-to-text transformer. *Journal of machine learning research*, 21: 1–67, 2020.

Raginsky, M., Rakhlin, A., Tsao, M., Wu, Y., and Xu, A. Information-theoretic analysis of stability and bias of learning algorithms. In *2016 IEEE Information Theory Workshop (ITW)*, pp. 26–30. IEEE, 2016.

Ranzato, M., Boureau, Y.-L., Cun, Y., et al. Sparse feature learning for deep belief networks. *Advances in neural information processing systems*, 20, 2007.

Salimans, T. and Kingma, D. P. Weight normalization: A simple reparameterization to accelerate training of deep neural networks. *Advances in neural information processing systems*, 29, 2016.

Saxe, A. M., Bansal, Y., Dapello, J., Advani, M., Kolchinsky, A., Tracey, B. D., and Cox, D. D. On the information bottleneck theory of deep learning. *Journal of Statistical Mechanics: Theory and Experiment*, 2019:124020, 2019.

Shamir, O., Sabato, S., and Tishby, N. Learning and generalization with the information bottleneck. *Theoretical Computer Science*, 411:2696–2711, 2010.

Shwartz-Ziv, R. and Tishby, N. Opening the black box of deep neural networks via information. *arXiv preprint arXiv:1703.00810*, 2017.

Siarohin, A., Sangineto, E., and Sebe, N. Whitening and coloring batch transform for gans. *arXiv preprint arXiv:1806.00420*, 2018.

Summers, C. and Dinneen, M. J. Four things everyone should know to improve batch normalization. *arXiv preprint arXiv:1906.03548*, 2019.

Tishby, N. and Zaslavsky, N. Deep learning and the information bottleneck principle. In *2015 ieee information theory workshop (itw)*, pp. 1–5. Ieee, 2015.

Tishby, N., Pereira, F. C., and Bialek, W. The information bottleneck method. *arXiv preprint physics/0004057*, 2000.

Touvron, H., Lavril, T., Izacard, G., Martinet, X., Lachaux, M.-A., Lacroix, T., Rozière, B., Goyal, N., Hambro, E., Azhar, F., et al. Llama: Open and efficient foundation language models. *arXiv preprint arXiv:2302.13971*, 2023a.

Touvron, H., Martin, L., Stone, K., Albert, P., Almahairi, A., Babaei, Y., Bashlykov, N., Batra, S., Bhargava, P., Bhosale, S., et al. Llama 2: Open foundation and fine-tuned chat models. *arXiv preprint arXiv:2307.09288*, 2023b.

Vaswani, A., Shazeer, N., Parmar, N., Uszkoreit, J., Jones, L., Gomez, A. N., Kaiser, Ł., and Polosukhin, I. Attention is all you need. *Advances in neural information processing systems*, 30, 2017.

Weng, X., Ni, Y., Song, T., Luo, J., Anwer, R. M., Khan, S., Khan, F. S., and Huang, L. Modulate your spectrum in self-supervised learning. *arXiv preprint arXiv:2305.16789*, 2023.

Wu, Y. and He, K. Group normalization. In *Proceedings of the European conference on computer vision (ECCV)*, pp. 3–19, 2018.

Xu, J., Sun, X., Zhang, Z., Zhao, G., and Lin, J. Understanding and improving layer normalization. *Advances in neural information processing systems*, 32, 2019.

Yuan, L., Chen, Y., Wang, T., Yu, W., Shi, Y., Jiang, Z.-H., Tay, F. E., Feng, J., and Yan, S. Tokens-to-token vit: Training vision transformers from scratch on imagenet. In *Proceedings of the IEEE/CVF international conference on computer vision*, pp. 558–567, 2021.

Zhang, B. and Sennrich, R. Root mean square layer normalization. *Advances in Neural Information Processing Systems*, 32, 2019.

Zhang, C., Bengio, S., Hardt, M., Recht, B., and Vinyals, O. Understanding deep learning requires rethinking generalization. *arXiv preprint arXiv:1611.03530*, 2016.

---

Zhang, D., Yin, J., Zhu, X., and Zhang, C. Network representation learning: A survey. *IEEE transactions on Big Data*, 6:3–28, 2018.

Zhao, J., Zhang, Z., Chen, B., Wang, Z., Anandkumar, A., and Tian, Y. Galore: Memory-efficient lilm training by gradient low-rank projection. *arXiv preprint arXiv:2403.03507*, 2024.

Zhu, J., Chen, X., He, K., LeCun, Y., and Liu, Z. Transformers without normalization. In *Proceedings of the Computer Vision and Pattern Recognition Conference*, pp. 14901–14911, 2025.

---

## A. IBNorm

### A.1. Comparison with Task-Irrelevant Information Compression Methods in Representation Learning

Prior works (Tishby et al., 2000; Tishby & Zaslavsky, 2015; Saxe et al., 2019; Hua et al., 2021; Weng et al., 2023; Hu et al., 2025) explore the IB theory and representation learning methods, such as whitening, and empirically shows how hidden layers with activation nonlinearities and whitening modules aiming to decorrelate features and stabilize training can compress task-irrelevant information.

While these findings provide valuable empirical insights, there are two notable gaps unaddressed: (1) they do not examine how normalization layers influence the decomposition of task-relevant and task-irrelevant mutual information within neural representations, and (2) they do not provide a theoretical framework for how to design the normalization following the IB framework to facilitate more informative and robust representations. Importantly, activation and normalization are conceptually and structurally distinct: In modern LLMs (e.g., LLaMA, GPT), nonlinear activations occur only in the gated branch of the MLP, and do not influence the representations within each transformer block. In these architectures, inserting  $\tanh$  as an “activation” would not propagate compression throughout the model, since the gating branch represents only one component of the block.

In contrast, IBNorm applies compression directly the normalization layer, which is invoked throughout the model—after each attention block and MLP block in LLMs. This placement ensures that compression systematically modulates the IB value of the representation at every layer, producing effects that cannot be achieved by modifying the activation function alone. In addition, recent studies on normalization module in Transformer (Zhu et al., 2025; Chen et al., 2025) replace variance-centric normalization layers with point-wise functions such as Dynamic Tanh, showing that the resulting performance gains arise primarily from improved generalization rather than increased fitting capacity. This observation is consistent with the IB principle underlying our work. Our proposed IBNorm is grounded on the IB-theoretic analysis of normalization and demonstrates how different IB-motivated compression operations shape higher-order statistics, aligning normalization behavior with the IB principle.

### A.2. Comparison with Training Pipelines Based on Explicit Information Bottleneck Objectives

Methods (Kolchinsky et al., 2019; Alemi et al., 2016; Belghazi et al., 2018) focus on estimating mutual information by parameterizing the IB principle with pretrained neural MI estimators and then guiding the training of deep learning models using the explicit estimated IB objective. These approaches typically rely on encoder-decoder architectures (e.g., VAEs), require large training datasets to train accurate and lightweight MI estimators before training the deep learning models, and introduce additional estimated MI-regularization loss functions during training the deep learning models. These components introduce extra hyperparameters, increase computational cost, and may lead to unstable optimization. Specifically, these approaches face two key limitations when applied to deep learning models, such as autoregressive LLMs where the sequential decoding process complicates the design and increases the inference cost of MI estimators, in practice:

**MI Neural Estimator Architecture and Computational Overhead:** These methods require additional MI neural estimators with architectural constraints alongside the main network, significantly increasing heavy inference computational cost and complicating optimization. In addition, designing such neural estimators is particularly difficult for autoregressive LLMs due to their sequential decoding characteristics.

**Sample Complexity:** Accurate MI estimation, as noted in MINE (Belghazi et al., 2018), requires large sample sizes, which is challenging for models with long-context inputs and requires heavy training cost.

IBNorm fills this gap by providing the first theoretical analysis of normalization under the IB principle. Specifically, IBNorm incorporates the IB principle within the normalization operation. It requires no auxiliary MI estimators, no additional IB-based training losses, and no architectural constraints. The compression operation introduced in IBNorm is not an external module but a theoretically grounded reformulation of normalization that increases the IB value of intermediate representations while adding minimal computational overhead.

We highlight the key advantages of IBNorm here:

**Systematic Theoretical Grounding:** We provide a theoretical analysis of widely used variance-centric normalization methods. This analysis motivates a principled mechanism for designing normalization layers that follow IB principle, as shown in Sec. 4.3.

---

**Computational Efficiency:** Unlike (Kolchinsky et al., 2019; Alemi et al., 2016; Belghazi et al., 2018), IBNorm does not rely on computationally heavy MI neural estimators or explicit IB regularizers, making it more efficient and stable during training. We include the comparison of training time and VRAM across IBNorm and baselines in Appendix C.8.

**Compatibility:** Probabilistic coding method like Structured Probabilistic Coding (SPC) (Hu et al., 2024) introduces an IB-inspired coding mechanism, but it is limited to encoder-only models and does not examine normalization layers. IBNorm is model-agnostic and can be directly integrated into Transformers (e.g., LLaMA, GPT-2) and CNNs (e.g., ResNet) without modifying the training pipeline, as demonstrated in Sec. 5.

### A.3. IBNorm Algorithm

Formally, given an activation input  $\mathbf{x}$ , IBNorm applies the following sequence of operations: first, the NAP operator  $\zeta$  partitions features in the same way as LayerNorm; next, a compression operator  $s_\lambda$  reduces nuisance variability; then, the NOP operator  $\psi$  standardizes activations; and finally, the NRR operator  $\eta$  rescales and shifts them:

$$\text{IBNorm}(\mathbf{x}; \lambda) \equiv \eta \circ \psi \circ s_\lambda \circ \zeta. \quad (13)$$

Here we summarize the IBNorm algorithmic steps in Algorithm 1. By construction, IBNorm goes beyond variance normalization: it acts as an *information filter*, enhancing sufficiency by retaining predictive information while improving minimality through compression of irrelevant information in the input. In this way, IBNorm bridges the gap between practical optimization benefits and information-theoretic optimality.

---

**Algorithm 1** IB-inspired normalization (IBNorm)

---

- 1: **Input:** Activations  $\mathbf{x} \in \mathbb{R}^{d \times m \times h \times w}$ , hyperparameter  $\lambda$
- 2: **Output:** Normalized activations  $\mathbf{y} \in \mathbb{R}^{d \times m \times h \times w}$
- 3: Normalization area partitioning (NAP):  $\hat{\mathbf{x}} \leftarrow \zeta(\mathbf{x})$
- 4: Compression operation:  $\tilde{\mathbf{x}} \leftarrow s_\lambda(\hat{\mathbf{x}})$
- 5: Normalization operation (NOP):  $\bar{\mathbf{x}} \leftarrow \psi(\tilde{\mathbf{x}})$
- 6: Normalization representation recovery (NRR):  $\hat{\mathbf{y}} \leftarrow \eta(\bar{\mathbf{x}})$
- 7: Reshape back:  $\mathbf{y} \leftarrow \zeta^{-1}(\hat{\mathbf{y}})$

---

## B. NormalNorm

We first provide the specific algorithm of NormalNorm in Algorithm 2.

**Power Transform.** Consider a random variable  $X$  from which a sample  $\mathbf{x} = \{x_i\}_{i=1}^H$  is obtained. The power transform  $g(\cdot; \lambda)$  gaussianizes  $\mathbf{x}$  by applying the following function for each  $x_i$ :

$$g(x_i; \lambda) = \begin{cases} \frac{(x_i+1)^\lambda - 1}{\lambda}, & x_i \geq 0, \lambda \neq 0 \\ \log(x_i + 1), & x_i \geq 0, \lambda = 0 \\ -\frac{(-x_i+1)^{2-\lambda} - 1}{2-\lambda}, & x_i < 0, \lambda \neq 2 \\ -\log(-x_i + 1), & x_i < 0, \lambda = 2, \end{cases} \quad (14)$$

where  $\lambda$  is a transformation parameter typically estimated from the data to make the transformed values approximately normally distributed.

The key design difference lies in how NormalNorm and IBNorm shape hidden activation distributions. NormalNorm aims to maximize the entropy of hidden activations by applying a power transform after standardization. In contrast, our proposed IBNorm follows the IB principle and shapes the activation distributions via a *compression operation* applied *before* standardization.

While NormalNorm also attempts to explicitly shape activation distributions, encouraging Gaussian-like features through the power transform with additive noise, this approach has several limitations: 1) In practice, we find that dynamically varying  $\lambda$  not only increases computational cost (see Appendix C.8), but can also lead to training instability due to numerical issues, especially in the setting of lower precision like bfloat16. 2) Furthermore, because the power transform modifies both the

---

first- and second-order statistics of the hidden activations, the resulting outputs after the NOP no longer have zero mean and unit variance. As a result, the network cannot fully benefit from traditional normalization techniques, such as improved training stability and scale invariance.

---

**Algorithm 2** Normal Normalization (Eftekhari & Papyan, 2025)

---

- 1: **Input:**  $u = \{u_i\}_{i=1}^N$
- 2: **Input:**  $y = \{y_i\}_{i=1}^N$
- 3: **Learnable Parameters:**  $\gamma, \beta$
- 4: **Noise Factor:**  $\xi \geq 0$
- Standardization:**
- 5:  $\hat{u} \leftarrow \frac{1}{N} \sum_{i=1}^N u_i$
- 6:  $\hat{\sigma}^2 \leftarrow \frac{1}{N} \sum_{i=1}^N (u_i - \hat{u})^2$
- 7:  $c_i \leftarrow \frac{u_i - \hat{u}}{\sqrt{\hat{\sigma}^2 + \epsilon}}$
- Power Transform and Scaled Additive Noise:**
- 8:  $x_i \leftarrow g(c_i; \hat{\lambda})$
- 9: with gradient tracking disabled:
- 10:  $\bar{x} = \frac{1}{N} \sum_{i=1}^N x_i$
- 11:  $s = \frac{1}{N} \sum_{i=1}^N |x_i - \bar{x}|$
- 12: sample  $z_i \sim \mathcal{N}(0, 1)$
- 13:  $v_i = x_i + z_i \cdot s \cdot \xi$
- Affine Transform:**
- 14:  $y_i \leftarrow \gamma \cdot v_i + \beta$

---

## C. Extended Empirical Results

### C.1. Results on LLM Leaderboard I

Table 6. Results of Llama models evaluated on LLM Leaderboard I.

Model	Normalization	ARC ( $\uparrow$ )	HellaSwag ( $\uparrow$ )	MMLU ( $\uparrow$ )	TruthfulQA ( $\uparrow$ )	Winogrande ( $\uparrow$ )	GSM8K ( $\uparrow$ )	AVG ( $\uparrow$ )
Llama 60M	LayerNorm	0.2150	0.2725	0.2557	0.4935	0.5075	0.0031	0.2912
	RMSNorm	0.2244	0.2783	0.2496	0.4761	0.5059	0.0023	0.2894
	NormalNorm	0.2270	0.2504	0.2295	0.4925	0.4957	0.0000	0.2825
	IBNorm-S	0.2631	0.2616	0.2526	0.4899	0.5028	0.0000	0.2950
	IBNorm-L	0.2568	0.2651	0.2689	0.4966	0.4854	0.0000	<b>0.2955</b>
	IBNorm-T	0.2270	0.2758	0.2620	0.4827	0.5099	0.0049	0.2937
Llama 130M	LayerNorm	0.2312	0.2795	0.2562	0.4754	0.5059	0.0042	0.2921
	RMSNorm	0.2210	0.2950	0.2494	0.4639	0.5154	0.0019	0.2911
	NormalNorm	0.2244	0.2684	0.2621	0.4797	0.5178	0.0027	0.2925
	IBNorm-S	0.2295	0.2950	0.2616	0.4698	0.5012	0.0027	0.2933
	IBNorm-L	0.2577	0.2697	0.2697	0.4892	0.4891	0.0019	0.2962
	IBNorm-T	0.2267	0.2900	0.2619	0.4949	0.5043	0.0042	<b>0.2970</b>
Llama 350M	LayerNorm	0.2355	0.3286	0.2579	0.4889	0.5225	0.0038	0.3062
	RMSNorm	0.2432	0.3155	0.2513	0.5201	0.4808	0.0038	0.3025
	NormalNorm	0.2398	0.3031	0.2618	0.4998	0.5107	0.0057	0.3035
	IBNorm-S	0.2363	0.3463	0.2620	0.4917	0.5149	0.0023	0.3089
	IBNorm-L	0.2619	0.3342	0.2692	0.4966	0.4949	0.0038	<b>0.3101</b>
	IBNorm-T	0.2598	0.3346	0.2623	0.4957	0.4970	0.0038	0.3089
Llama 1B	LayerNorm	0.2364	0.3711	0.2580	0.4882	0.5226	0.0064	0.3138
	RMSNorm	0.2517	0.3593	0.2522	0.5035	0.5093	0.0045	0.3134
	NormalNorm	0.2244	0.3183	0.2713	0.4961	0.5170	0.0038	0.3051
	IBNorm-S	0.2551	0.3749	0.2636	0.4923	0.5188	0.0057	0.3184
	IBNorm-L	0.2632	0.3725	0.2691	0.4945	0.4980	0.0099	0.3179
	IBNorm-T	0.2654	0.3809	0.2663	0.4952	0.5075	0.0042	<b>0.3199</b>

Table 7. Results of GPT-2 models evaluated on LLM Leaderboard I.

Model	Normalization	ARC ( $\uparrow$ )	HellaSwag ( $\uparrow$ )	MMLU ( $\uparrow$ )	TruthfulQA ( $\uparrow$ )	Winogrande ( $\uparrow$ )	GSM8K ( $\uparrow$ )	AVG ( $\uparrow$ )
GPT-2 124M	LayerNorm	0.2483	0.2667	0.2371	0.4868	0.4933	0.0000	0.2887
	RMSNorm	0.2551	0.2540	0.2373	0.4848	0.4838	0.0008	0.2860
	NormalNorm	0.2645	0.0000	0.2632	0.2457	0.4890	0.4941	0.2927
	IBNorm-S	0.2690	0.2558	0.2458	0.4846	0.5053	0.0000	0.2934
	IBNorm-L	0.2756	0.2577	0.2689	0.4859	0.4933	0.0008	<b>0.2970</b>
	IBNorm-T	0.2734	0.2569	0.2394	0.4835	0.5178	0.0004	0.2952
GPT-2 355M	LayerNorm	0.2637	0.2772	0.2485	0.4945	0.5051	0.0011	0.2983
	RMSNorm	0.2643	0.2673	0.2518	0.4951	0.4917	0.0000	0.2950
	NormalNorm	0.2601	0.2683	0.2549	0.4948	0.4949	0.0000	0.2955
	IBNorm-S	0.2781	0.2679	0.2581	0.4955	0.5072	0.0000	0.3011
	IBNorm-L	0.2813	0.2681	0.2693	0.4964	0.5058	0.0000	<b>0.3035</b>
	IBNorm-T	0.2819	0.2693	0.2532	0.4972	0.5185	0.0011	<b>0.3035</b>

## C.2. Results with Statistical Significance

Table 8. Results of Llama models evaluated on LLM Leaderboard I and II.

Model	Normalization	Leaderboard I ( $\uparrow$ )	Leaderboard II ( $\uparrow$ )
Llama 60M	LayerNorm	0.2910 $\pm$ 0.0020	0.1922 $\pm$ 0.0033
	RMSNorm	0.2895 $\pm$ 0.0027	0.1927 $\pm$ 0.0038
	NormalNorm	0.2823 $\pm$ 0.0029	0.1895 $\pm$ 0.0053
	IBNorm-L	<b>0.2955 <math>\pm</math> 0.0022</b>	<b>0.2055 <math>\pm</math> 0.0031</b>
Llama 130M	LayerNorm	0.2919 $\pm$ 0.0021	0.1942 $\pm$ 0.0035
	RMSNorm	0.2913 $\pm$ 0.0027	0.1940 $\pm$ 0.0039
	NormalNorm	0.2918 $\pm$ 0.0031	0.1927 $\pm$ 0.0055
	IBNorm-T	<b>0.2973 <math>\pm</math> 0.0024</b>	<b>0.2133 <math>\pm</math> 0.0037</b>
Llama 350M	LayerNorm	0.3062 $\pm$ 0.0020	0.2003 $\pm$ 0.0037
	RMSNorm	0.3025 $\pm$ 0.0028	0.2010 $\pm$ 0.0041
	NormalNorm	0.3035 $\pm$ 0.0033	0.1962 $\pm$ 0.0058
	IBNorm-L	<b>0.3101 <math>\pm</math> 0.0021</b>	<b>0.2116 <math>\pm</math> 0.0047</b>
Llama 1B	IBNorm-T	<b>0.3089 <math>\pm</math> 0.0022</b>	<b>0.2140 <math>\pm</math> 0.0050</b>
	LayerNorm	0.3138 $\pm$ 0.0024	0.2053 $\pm$ 0.0042
	RMSNorm	0.3134 $\pm$ 0.0030	0.2019 $\pm$ 0.0048
	NormalNorm	0.3051 $\pm$ 0.0049	0.2006 $\pm$ 0.0067
	IBNorm-T	<b>0.3199 <math>\pm</math> 0.0027</b>	<b>0.2162 <math>\pm</math> 0.0053</b>

Table 9. Results of GPT-2 models evaluated on LLM Leaderboard I and II.

Model	Normalization	Leaderboard I ( $\uparrow$ )	Leaderboard II ( $\uparrow$ )
GPT-2 124M	LayerNorm	0.2888 $\pm$ 0.0017	0.1889 $\pm$ 0.0021
	RMSNorm	0.2861 $\pm$ 0.0019	0.1883 $\pm$ 0.0025
	NormalNorm	0.2923 $\pm$ 0.0027	0.1983 $\pm$ 0.0031
	IBNorm-L	<b>0.2969 <math>\pm</math> 0.0022</b>	<b>0.2068 <math>\pm</math> 0.0025</b>
GPT-2 355M	LayerNorm	0.2978 $\pm$ 0.0024	0.1920 $\pm$ 0.0037
	RMSNorm	0.2949 $\pm$ 0.0031	0.1948 $\pm$ 0.0042
	NormalNorm	0.2953 $\pm$ 0.0035	0.1985 $\pm$ 0.0044
	IBNorm-L	<b>0.3034 <math>\pm</math> 0.0028</b>	<b>0.2125 <math>\pm</math> 0.0048</b>

**Discussion of Failure Cases.** Our evaluation reveals distinct performance characteristics across different task types. While IBNorm consistently improves performance on tasks involving factual retrieval and general language modeling, it achieves suboptimal performance on reasoning-intensive benchmarks such as BBH, GPQA, and MMLU-PRO. These benchmarks place substantial demands on the model’s ability to preserve and integrate intermediate representations across multiple inference steps, particularly in deeper layers. Qualitative analysis shows that models trained with IBNorm tend to produce more concise rationales compared to LayerNorm and RMSNorm baselines. In many challenging cases, the model correctly identifies the key premises and relevant entities, but intermediate inference steps are less explicitly represented, which can affect performance on tasks requiring extended deductive chains. To further characterize this behavior, we examine the entropy of hidden representations and output distributions. We find that IBNorm consistently induces lower activation and token-level entropy in deeper layers for reasoning tasks, indicating a more compact representational structure.

From an information-theoretic perspective, this behavior reflects the inherent trade-off between minimality and sufficiency in the information bottleneck objective, regulated by the hyperparameter  $\lambda$ . Stronger compression favors representations that are highly predictive of the target output while minimizing redundancy, which is advantageous for retrieval-oriented tasks but may be less aligned with reasoning benchmarks that benefit from maintaining high-entropy intermediate latent states. These observations motivate a layer-dependent normalization strategy as a promising direction for future work. Applying IBNorm in early or intermediate layers can encourage informative representations, while retaining variance-based normalization in deeper layers may help preserve the representational entropy and flexibility necessary for multi-step reasoning.

### C.3. Ablation Study on Normalization Structure

Table 10. Ablation study of Llama 60M evaluated on LLM Leaderboard I.

Normalization	ARC (↑)	HellaSwag (↑)	MMLU (↑)	TruthfulQA (↑)	Winogrande (↑)	GSM8K (↑)	AVG (↑)
IBNorm-S*	0.2661	0.2698	0.2542	0.4788	0.5012	0.0011	0.2952
IBNorm-S**	0.2587	0.2570	0.2535	0.4750	0.4822	0.0023	0.2881
IBNorm-T*	0.2518	0.2658	0.2570	0.4879	0.4988	0.0004	0.2936
IBNorm-T**	0.2261	0.2562	0.2472	0.4740	0.4941	0.0008	0.2831
IBNorm-L*	0.2483	0.2615	0.2389	0.5029	0.4886	0.0030	0.2905
IBNorm-L**	0.2435	0.2606	0.2407	0.4743	0.4957	0.0008	0.2859

Table 11. Ablation study of Llama 60M evaluated on LLM Leaderboard II.

Normalization	IFEval (↑)	BBH (↑)	MATH (↑)	Leaderboard II			AVG (↑)	Leaderboard I AVG (↑)
				GPQA (↑)	MUSR (↑)	MMLU-PRO (↑)		
IBNorm-S*	0.1626	0.2646	0.0000	0.2876	0.3609	0.1114	0.1978	0.2952
IBNorm-S**	0.1376	0.2946	0.0000	0.2776	0.3460	0.1114	0.1945	0.2881
IBNorm-T*	0.1372	0.2880	0.0000	0.2801	0.3519	0.1166	0.1956	0.2936
IBNorm-T**	0.1272	0.2980	0.0000	0.2701	0.3519	0.1166	0.1940	0.2831
IBNorm-L*	0.1374	0.2941	0.0000	0.2793	0.3505	0.1190	0.1967	0.2905
IBNorm-L**	0.1374	0.2841	0.0000	0.2693	0.3505	0.1190	0.1934	0.2859

### C.4. Ablation Study on $\lambda$

Table 12. Ablation study of Llama 60M with normalization using different  $\lambda$  evaluated on LLM Leaderboard I.

Normalization	$\lambda$	ARC (↑)	HellaSwag (↑)	MMLU (↑)	TruthfulQA (↑)	Winogrande (↑)	GSM8K (↑)	AVG (↑)
IBNorm-S	0.5	0.2227	0.2641	0.2478	0.4948	0.5046	0.0045	0.2898
	4	0.2393	0.2665	0.2496	0.5033	0.5078	0.0049	<b>0.2952</b>
	8	0.2270	0.2647	0.2579	0.4984	0.4958	0.0072	0.2918
IBNorm-L	0.5	0.2193	0.2781	0.2501	0.4892	0.4767	0.0045	0.2863
	4	0.2568	0.2651	0.2689	0.4966	0.4854	0.0000	<b>0.2955</b>
	8	0.2722	0.2692	0.2293	0.4853	0.4964	0.0000	0.2921
IBNorm-T	0.5	0.2243	0.2644	0.2692	0.4846	0.4862	0.0000	0.2881
	4	0.2270	0.2758	0.2620	0.4827	0.5099	0.0049	<b>0.2937</b>
	8	0.2274	0.2645	0.2519	0.4923	0.5028	0.0000	0.2898

Table 13. Ablation study of Llama 60M with normalization using different  $\lambda$  evaluated on LLM Leaderboard II.

Normalization	$\lambda$	IFEval (↑)	BBH (↑)	MATH (↑)	Leaderboard II			AVG (↑)	Leaderboard I AVG (↑)
					GPQA (↑)	MUSR (↑)	MMLU-PRO (↑)		
IBNorm-S	0.5	0.1687	0.2894	0.0008	0.2592	0.3519	0.1162	0.1977	0.2898
	4	0.1781	0.2977	0.0000	0.2501	0.3571	0.1091	<b>0.1987</b>	<b>0.2952</b>
	8	0.1623	0.2947	0.0008	0.2606	0.3515	0.1185	0.1981	0.2918
IBNorm-L	0.5	0.1577	0.2968	0.0000	0.2710	0.3690	0.1162	0.2018	0.2863
	4	0.1899	0.3001	0.0000	0.2772	0.3519	0.1137	<b>0.2055</b>	<b>0.2955</b>
	8	0.1364	0.2888	0.0000	0.2450	0.3452	0.1132	0.1881	0.2921
IBNorm-T	0.5	0.1761	0.3024	0.0000	0.2492	0.3469	0.1158	0.1984	0.2881
	4	0.1754	0.3013	0.0008	0.2668	0.3598	0.1110	<b>0.2025</b>	<b>0.2937</b>
	8	0.1753	0.2933	0.0000	0.2559	0.3631	0.1156	0.2005	0.2898

Table 14. Ablation study of GPT-2 124M with normalization using different  $\lambda$  evaluated on LLM Leaderboard I.

Normalization	$\lambda$	ARC ( $\uparrow$ )	HellaSwag ( $\uparrow$ )	MMLU ( $\uparrow$ )	TruthfulQA ( $\uparrow$ )	Winogrande ( $\uparrow$ )	GSM8K ( $\uparrow$ )	AVG ( $\uparrow$ )
IBNorm-T	0.5	0.2652	0.2634	0.2512	0.4896	0.5092	0.0000	0.2964
	4	0.2819	0.2693	0.2532	0.4972	0.5185	0.0011	<b>0.3035</b>
	8	0.2794	0.2660	0.2522	0.4903	0.5037	0.0000	0.2986

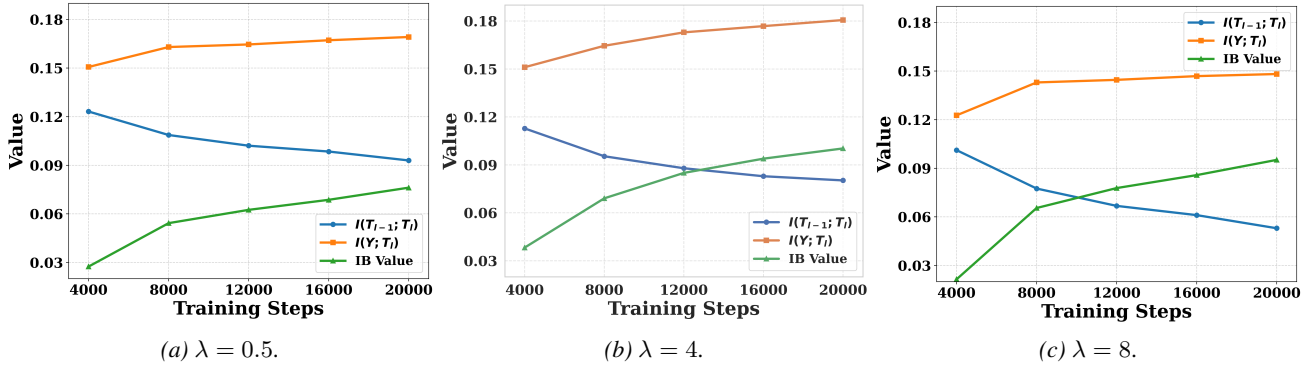


Figure 3. Evolution of predictive information  $\hat{I}(Y; T_l)$ , task-nuisance information  $\hat{I}(T_{l-1}; T_l)$ , and the token-level IB value during training of Llama-130M on C4, using IBNorm-T across different hyperparameters  $\lambda = 0.5, 4, 8$ . Results are reported on the test set.

As shown in Figure 3, we find: 1) Under-compression ( $\lambda = 0.5$ ) fails to sufficiently suppress task-irrelevant information, leading to suboptimal IB tradeoffs. 2) Over-compression ( $\lambda = 8$ ) starts to suppress task-relevant information, harming predictive performance. 3) Moderate compression ( $\lambda = 4$ ) achieves the best IB value, effectively removing nuisance factors while preserving task-useful information.

### C.5. Extended Results on ImageNet

In addition to the results for ViT in Tab. 3, we conduct ViT experiments following the ViT-S/16 and ViT-B/16 settings (Yuan et al., 2021), with details provided in Appendix F.2.

Table 15. Accuracy (%) of ViT-S/16 and ViT-B/16 on image classification tasks. We present LayerNorm’s results on Vision Transformer (ViT) because it performs much better than BatchNorm.

Normalization	ViT-S/16 on ImageNet		ViT-B/16 on ImageNet	
	Top-1	Top-5	Top-1	Top-5
BatchNorm	—	—	—	—
LayerNorm	78.25	94.12	81.09	95.57
RMSNorm	78.19	93.98	81.06	95.50
NormalNorm	78.77	94.21	81.03	95.46
IBNorm-S	80.23	94.94	82.53	95.97
IBNorm-L	80.57	95.12	83.69	96.43
IBNorm-T	<b>80.76</b>	<b>95.21</b>	<b>83.71</b>	<b>96.49</b>

Table 16. Accuracy (%) on CIFAR-10 with ResNet18. We report BatchNorm’s results since it significantly outperforms LayerNorm on CNNs.

Normalization	Top-1	Top-5
BatchNorm	93.65	99.85
IterNorm	94.48	99.86
LayerNorm	—	—
RMSNorm	—	—
NormalNorm	94.01	99.86
IBNorm-S	95.49	99.85
IBNorm-L	<b>95.57</b>	<b>99.87</b>
IBNorm-T	95.51	99.83

### C.6. The Effect of Compression Operation in IBNorm

We instantiate three representative forms of the compression function  $f_\lambda$ :

$$f_\lambda(|x_i - \mu|) = |x_i - \mu|/\lambda, \quad (\text{IBNorm-S, linear compression})$$

$$f_\lambda(|x_i - \mu|) = \ln(1 + |x_i - \mu|/\lambda), \quad (\text{IBNorm-L, logarithmic compression})$$

$$f_\lambda(|x_i - \mu|) = \tanh(|x_i - \mu|/\lambda). \quad (\text{IBNorm-T, hyperbolic tangent compression})$$

These choices capture complementary compression behaviors. Specifically, IBNorm-S provides a linear baseline, IBNorm-L yields progressively stronger suppression of large activations, and IBNorm-T enforces a hard saturation effect on extreme values. Together, they span the spectrum from mild to strong tail suppression while sharing the desirable properties of boundedness and monotonicity. While other monotonic compression functions are possible, we provide these three forms to demonstrate the range of behaviors and provide a principled comparison.

The bounded compression property requires

$$0 \leq f_\lambda(r) \leq \alpha_\lambda r, \quad \forall r \geq 0, \quad \alpha_\lambda \in [0, 1].$$

To determine  $\alpha_\lambda$ , we analyze the ratio  $f_\lambda(r)/r$ .

**Linear.** For  $f_\lambda(r) = r/\lambda$ ,

$$\frac{f_\lambda(r)}{r} = \frac{1}{\lambda}, \quad \forall r > 0,$$

thus  $\alpha_\lambda = 1/\lambda$ .

**Logarithmic.** For  $f_\lambda(r) = \log(1 + r/\lambda)$ ,

$$\frac{f_\lambda(r)}{r} = \frac{\log(1 + r/\lambda)}{r},$$

which is monotonically decreasing in  $r$  and attains its maximum at  $r \rightarrow 0$ :

$$\lim_{r \rightarrow 0} \frac{\log(1 + r/\lambda)}{r} = \frac{1}{\lambda}.$$

Hence  $\alpha_\lambda = 1/\lambda$ .

**Hyperbolic tangent.** For  $f_\lambda(r) = \tanh(r/\lambda)$ , the ratio

$$\frac{f_\lambda(r)}{r}$$

is maximized as  $r \rightarrow 0$ , giving

$$\lim_{r \rightarrow 0} \frac{\tanh(r/\lambda)}{r} = \frac{1}{\lambda}.$$

Thus  $\alpha_\lambda = 1/\lambda$ .

In conclusion, for these functionals, the compression ratio  $\alpha_\lambda$  in Eqn. (7) is given by  $\alpha_\lambda = 1/\lambda$ , which guarantees the bounded compression property whenever  $\lambda \geq 1$ . Compression operations in IBNorm compress the tail of activations while adjusting higher-order statistics.

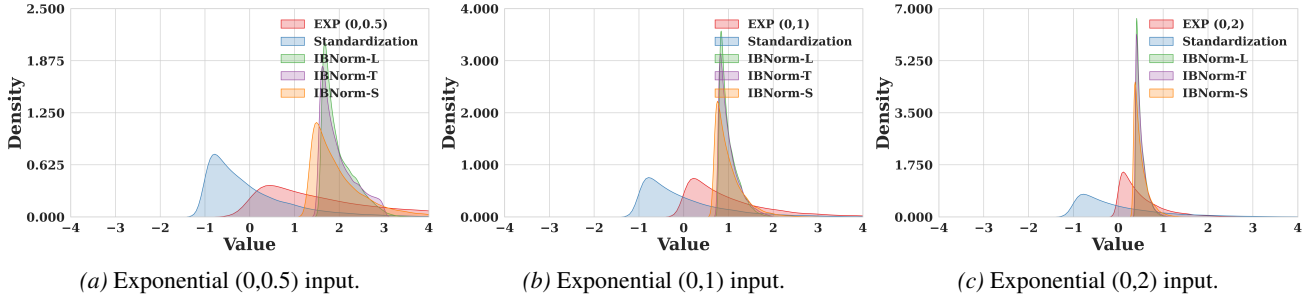


Figure 4. Comparison of kernel density estimation across different compression operation (Standardization, IBNorm-L ( $\lambda = 4$ ), IBNorm-T ( $\lambda = 4$ ), IBNorm-S ( $\lambda = 3$ )) given Exponential distribution inputs with mean 0 and different lambdas. Compression operations in IBNorm compress the tail in the activations and adjust the higher-order statistics.

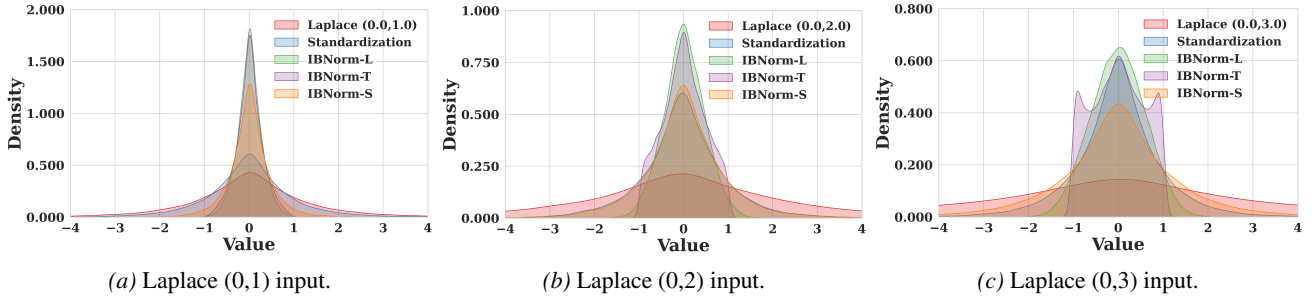


Figure 5. Comparison of kernel density estimation across different compression operation (Standardization, IBNorm-L ( $\lambda = 4$ ), IBNorm-T ( $\lambda = 4$ ), IBNorm-S ( $\lambda = 3$ )) given Laplace distribution inputs with mean 0 and different scales. Compression operations in IBNorm compress the tail in the activations and adjust the higher-order statistics.

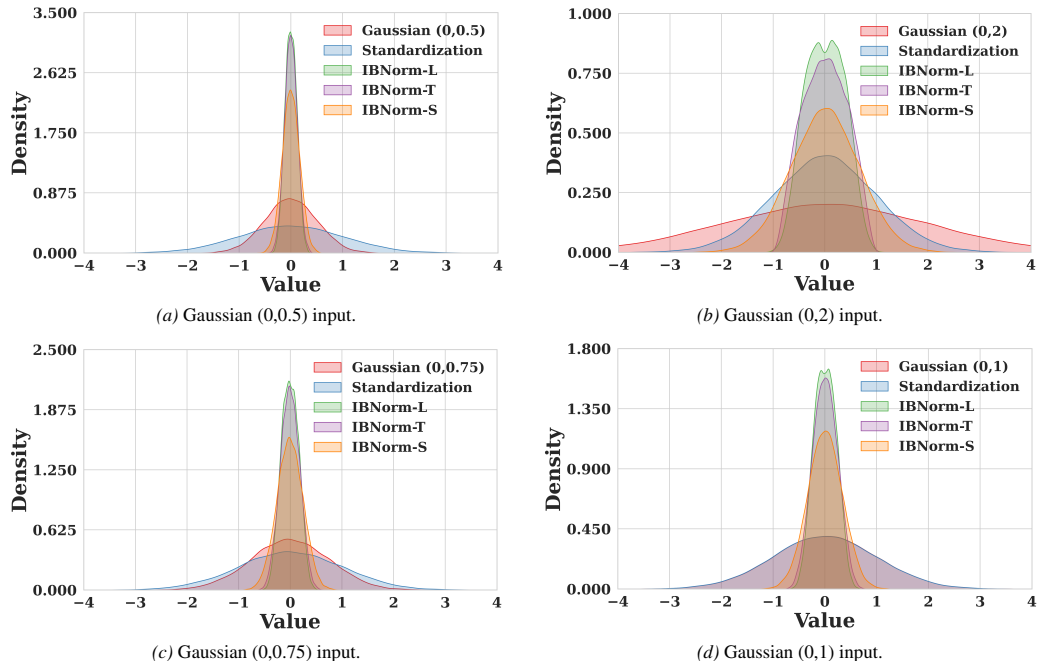


Figure 6. Comparison of kernel density estimation across different compression operation (Standardization, IBNorm-L ( $\lambda = 4$ ), IBNorm-T ( $\lambda = 4$ ), IBNorm-S ( $\lambda = 3$ )) given Gaussian distribution inputs with mean 0 and different variance. Compression operations in IBNorm compress the tail in the activations and adjust the higher-order statistics.

**Distinction of IBNorm-S, IBNorm-L, and IBNorm-T** IBNorm-S, IBNorm-L, and IBNorm-T are three types of IBNorm, which satisfy the compression property. Compression operations in IBNorm compress the tail of activations while adjusting higher-order statistics. IBNorm-L, IBNorm-T, and IBNorm-S exhibit different abilities to compress the tails of activations as shown in Figures 4, 5, and 6. These differences in how aggressively each function compresses activation tails further lead to the distinction in the induced entropy of the output distribution. Because all three satisfy IB constraints, their IB curves (predictive MI, nuisance MI, token-level IB value) follow similar trends during training, making it difficult to distinguish their own characteristics purely from the IB framework. For this reason, we provide an additional quantitative analysis using kernel density entropy, which directly reflects how much information each compression function filters.

Specifically, to illustrate the distinct compression behaviors of IBNorm-S, IBNorm-L, and IBNorm-T, we compute the entropy of the kernel density estimate (KDE) of activations after applying each variant (with the same hyperparameter  $\lambda = 4$  under different input distributions. For an input Gaussian  $\mathcal{N}(0, 2)$  with entropy 1.768, the resulting KDE entropies are 1.695 for IBNorm-S, 1.530 for IBNorm-L, and 1.302 for IBNorm-T. Similarly, for an input Gaussian  $\mathcal{N}(0, 1)$  with entropy 1.418, the corresponding output entropies are 1.352 for IBNorm-S, 1.263 for IBNorm-L, and 1.192 for IBNorm-T. These results indicate that IBNorm-S performs the mildest compression, IBNorm-L achieves stronger compression, and IBNorm-T is the most aggressive in reducing entropy. This analysis highlights the distinct statistical effects of the three variants on latent representations.

Beyond compression strength, we observe differences in robustness. As shown in Tables 4 and 12, IBNorm-S is less sensitive to variations in the hyperparameter  $\lambda$  compared to IBNorm-L and IBNorm-T. Similarly, ablation studies on the normalization structure shown in Tables 5 and 10 indicate that IBNorm-S is more robust to the ordering of the IB compression and standardization operations.

At the task level, performance differences align with these compression characteristics. Across diverse medium-scale LLMs (Llama 130M-1B and GPT 355M), IBNorm-S generally achieves the worst performance among the three IBNorm variants on evaluation tasks in Tables 1 and 6, reflecting its mildest compression. For challenging tasks, such as BBH and GPQA, the stronger compression applied by IBNorm-L can lead to improved performance, suggesting that mild compression can better support reasoning and generalization in difficult tasks.

### C.7. Estimated Mutual Information Quantities and Token-level IB Value across Training

We track the evolution of three mutual information quantities during training: predictive information  $\hat{I}(Y; T_l)$ , task-nuisance information  $\hat{I}(T_{l-1}; T_l)$ , and their token-level IB value  $\hat{I}(Y; T_l) - \hat{I}(T_{l-1}; T_l)$ . These quantities are measured throughout training on test dataset for Llama-130M and GPT-2 (124M) on C4 and OpenWebText, respectively. The details in token-level IB value calculation are in Appendix G.

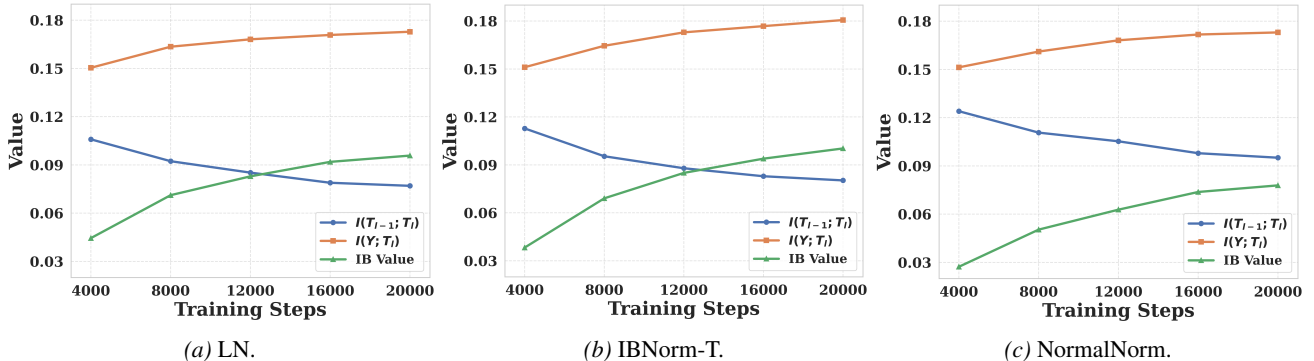


Figure 7. Evolution of predictive information  $\hat{I}(Y; T_l)$ , task-nuisance information  $\hat{I}(T_{l-1}; T_l)$ , and the token-level IB value during training of Llama-130M on C4, using LN, IBNorm-T, and NormalNorm. Results are reported on the test set.

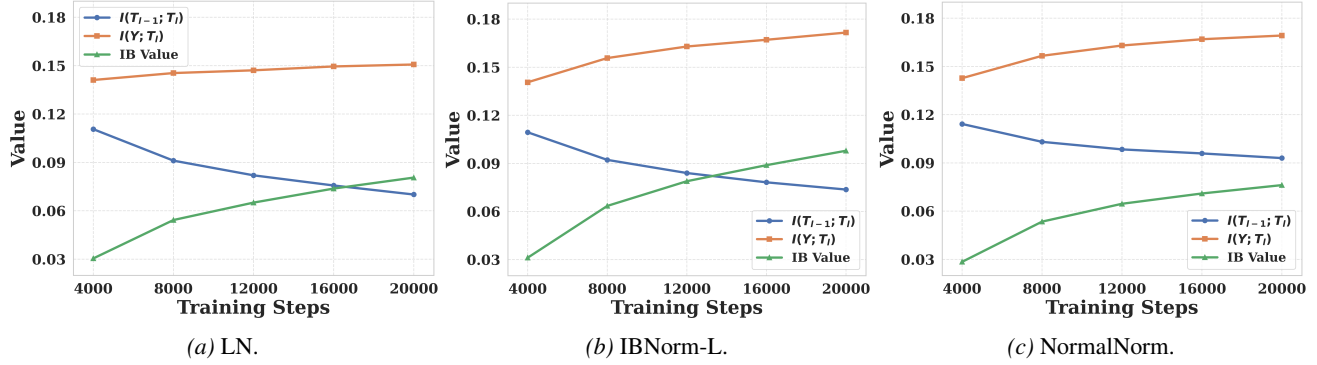


Figure 8. Evolution of predictive information  $\hat{I}(Y; T_l)$ , task-nuisance information  $\hat{I}(T_{l-1}; T_l)$ , and the token-level IB value during training of GPT-2 (124M) on OpenWebText, using LN, IBNorm-L, and NormalNorm. Results are reported on the test set.

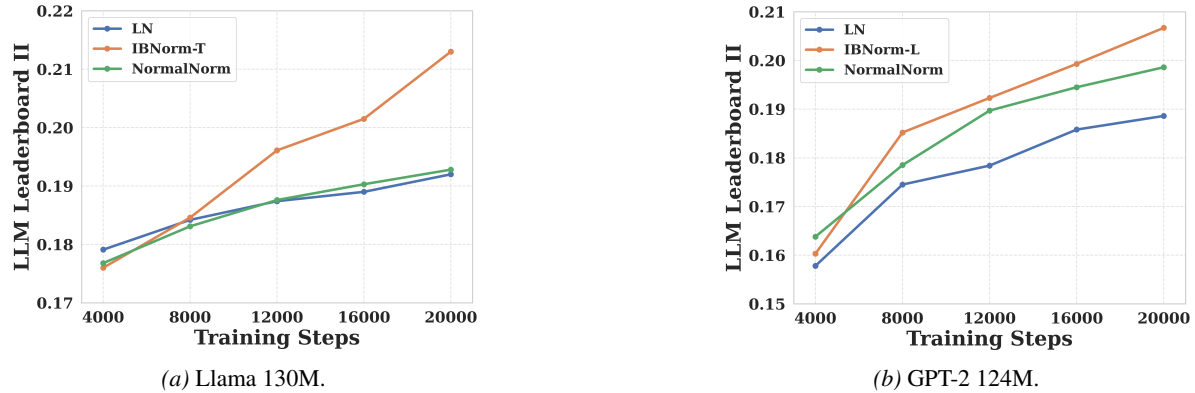


Figure 9. Evaluation of Llama 130M and GPT-2 124M trained with LN, IBNorm-L, NormalNorm on LLM Leaderboard II across training.

As shown in Figs. 7, 8, and 9, these results demonstrate that IBNorm encourages representations that retain task-relevant information while suppressing irrelevant task-nuisance information, providing an explanation for the observed empirical gains.

### C.8. Discussion on Training Time and Computational Overhead

IBNorm introduces only a single compression operation per normalization layer. Consequently, it does not incur significant computational overhead or cause numerical stability issues, even for larger models. Training time and memory usage of IBNorm remain comparable to standard variance-centric normalization methods such as LayerNorm or RMSNorm.

We report the training time and total VRAM usage for LLaMA-60M under the same global batch size 512 and local batch size 64, trained on 4× L40-S GPUs with 20000 training steps:

Table 17. Training time and VRAM usage for different normalization methods on LLaMA-60M.

Normalization	Training Time (↓)	Total VRAM (↓)
LayerNorm	1h 54min	95,944 MiB
RMSNorm	2h 15min	102,601 MiB
NormalNorm	3h 38min	139,207 MiB
IBNorm-S	2h 14min	102,460 MiB
IBNorm-L	2h 17min	106,371 MiB
IBNorm-T	2h 14min	104,853 MiB

We report the training time and total VRAM usage for LLaMA-1B under the same global batch size 512 and local batch size 8, trained on  $4 \times$  L40-S GPUs with 100000 training steps:

Table 18. Training time and VRAM usage for different normalization methods on LLaMA-1B.

Normalization	Training Time (↓)	Total VRAM (↓)
LayerNorm	176h 02min	99,832 MiB
RMSNorm	190h 58min	110,574 MiB
NormalNorm	246h 06min	162,088 MiB
IBNorm-S	194h 29min	115,920 MiB
IBNorm-L	190h 02min	106,484 MiB
IBNorm-T	188h 41min	106,481 MiB

## D. Details of Other Terms

We have

$$\begin{aligned}
& G(\sigma_{H_1|X}, \sigma_{H_1|Y}, \sigma_{p_1|X}, \sigma_{p_1|Y}, \mu_{p_1|X}, \mu_{p_1|Y}) \\
&= C_1 \sqrt{\frac{\sigma_{H_1|X}}{M}} + C_1 \sqrt{\frac{\sigma_{H_1|Y}}{M}} + \sum_y p(y) \int_{\tilde{\mathcal{T}}_1} \phi(\sqrt{\sigma_{p_1|Y}}) dt + \beta \sum_x p(x) \int_{\tilde{\mathcal{T}}_1} \phi(\sqrt{\sigma_{p_1|X}}) dt \\
&+ (\beta + 2) \int_{\tilde{\mathcal{T}}_1} \phi\left(C_1 \sqrt{\frac{\sigma_{H_1|X}}{M}}\right) p_{\tilde{T}_1}(t) dt + \sum_y p(y) \int_{\tilde{\mathcal{T}}_1} \phi(\mu_{p_1|Y}) dt + \beta \sum_x p(x) \int_{\tilde{\mathcal{T}}_1} \phi(\mu_{p_1|X}) dt \\
&+ (\beta + 1) \int_{\tilde{\mathcal{T}}_1} \sum_x p(x) [\phi(\sqrt{\sigma_{p_1|X}}) + \phi(\mu_{p_1|X})] dt,
\end{aligned}$$

where

$$\begin{aligned}
\sigma_{H_1|X} &:= V(H(\tilde{T}_1|X)) = |\mathcal{X}|V(H(\tilde{T}_1|X)), & \sigma_{H_1|Y} &:= V(H(\tilde{T}_1|Y)) = |\mathcal{Y}|V(H(\tilde{T}_1|Y)), \\
\sigma_{p_1|X} &:= V(p(\tilde{T}_1|X)) = |\mathcal{X}|V(p(\tilde{T}_1|X)), & \sigma_{p_1|Y} &:= V(p(\tilde{T}_1|Y)) = |\mathcal{Y}|V(p(\tilde{T}_1|Y)), \\
\mu_{p_1|X} &:= \mathbb{E}[p(\tilde{T}_1|X)], & \mu_{p_1|Y} &:= \mathbb{E}[p(\tilde{T}_1|Y)],
\end{aligned}$$

and

$$C_1 = 2 + \sqrt{2 \log((|\mathcal{Y}| + 2)/\delta)}.$$

In addition, we have the optimum-dependent term:

$$\begin{aligned}
Q(\tilde{T}_1^*) &= (2 + \sqrt{2 \log((|\mathcal{Y}| + 2)/\delta)}) \sqrt{\frac{V(H(\tilde{T}_1^*|Y))}{M}} \\
&+ \beta(2 + \sqrt{2 \log((|\mathcal{Y}| + 2)/\delta)}) \sqrt{\frac{V(H(\tilde{T}_1^*|X))}{M}} \\
&+ (\beta + 2) \int_{\tilde{\mathcal{T}}_1^*} \phi\left((2 + \sqrt{2 \log((|\mathcal{Y}| + 2)/\delta)}) \sqrt{\frac{V(p(\tilde{T}_1^*|X))}{M}}\right) p_{\tilde{T}_1^*}(t) dt \\
&+ \sum_y p(y) \int_{\tilde{\mathcal{T}}_1} \phi(p_{\tilde{T}_1^*|Y}(t|y)) dt + \beta \sum_x p(x) \int_{\tilde{\mathcal{T}}_1} \phi(p_{\tilde{T}_1^*|X}(t|x)) dt + (\beta + 1) \int_{\tilde{\mathcal{T}}_1} \phi(p(\tilde{T}_1^*)) dt \\
&+ (\beta + 1) \int_{\tilde{\mathcal{T}}_1} \sum_x p(x) \phi(p_{\tilde{T}_1^*|X}(t|x)) dt
\end{aligned}$$

## E. Proof

### E.1. Proof for Theorem 1

**Theorem.** For any hyperparameter  $\beta \in [0, 1]$  and the sample set  $S \sim \mathbb{P}(X, Y)$  of size  $M$ , we have

$$\widehat{IB}_S(T_{IB}) \geq \widehat{IB}_S(T_s) \quad \text{almost surely.}$$

*Proof.* Given the dataset  $S \sim \mathbb{P}_{X,Y}$  with size  $M$  and one-layer neural networks,  $f_1 = \Phi_1 \circ h$ . Because  $\eta$  is linear and invertible, it does not affect the mutual information terms (Hjelm et al., 2018; Ash & Doléans-Dade, 2000); therefore, it suffices to analyze the intermediate features  $\tilde{T}_s := \psi \circ \zeta \circ h(X)$  and  $\tilde{T}_{IB} := \psi \circ s_\lambda \circ \zeta \circ h(X)$ . We analyze the IB value of intermediate features  $\tilde{T}_1 := \psi \circ \zeta \circ h(X)$  in a general setting given a network  $f$ . First, we define the empirical gap  $\Delta_S(\tilde{T}_1; \tilde{T}_1^*)$  between the IB bottleneck derived from arbitrary representation  $\tilde{T}_1$  and the IB-optimum representation  $\tilde{T}_1^*$ , i.e.

$$\Delta_S(\tilde{T}_1; \tilde{T}_1^*) = |\hat{I}(Y; \tilde{T}_1) - \beta \hat{I}(\tilde{T}_0; \tilde{T}_1) - (\hat{I}(Y; \tilde{T}_1^*) - \beta \hat{I}(\tilde{T}_0^*; \tilde{T}_1^*)|, \quad (15)$$

where  $\tilde{T}_0 = \tilde{T}_0^* = X$ .

We prove  $\widehat{\text{IB}}_1 \geq \widehat{\text{IB}}_2$  by showing that  $\Delta_S(\tilde{T}_{IB}; \tilde{T}_1^*) \leq \Delta_S(\tilde{T}_s; \tilde{T}_1^*)$ .

**Lemma 3.** *Given a fixed trade-off hyperparameter  $\beta > 0$  and a confidence parameter  $\delta \in (0, 1)$ , the following holds with probability at least  $1 - \delta$  over any sample set  $S \sim \mathbb{P}(X, Y)$  with size  $M$ : for any representation  $\tilde{T}_1 \in \tilde{\mathcal{T}}_1$ ,*

$$\Delta_S(\tilde{T}_1; \tilde{T}_1^*) \leq G(\sigma_{H_1|X}, \sigma_{H_1|Y}, \sigma_{p_1|X}, \sigma_{p_1|Y}, \mu_{p_1|X}, \mu_{p_1|Y}) + Q(\tilde{T}_1^*). \quad (16)$$

where  $G(\cdot)$  is a monotonically increasing function with its arguments. Specifically,  $\sigma_{H_1|X} := \mathbb{V}(H(\tilde{T}_1|X))$ ,  $\sigma_{H_1|Y} := \mathbb{V}(H(\tilde{T}_1|Y))$ ,  $\sigma_{p_1|X} := \mathbb{V}(p(\tilde{T}_1|X))$ ,  $\sigma_{p_1|Y} := \mathbb{V}(p(\tilde{T}_1|Y))$ ,  $\mu_{p_1|X} := \mathbb{E}[p(\tilde{T}_1|X)]$ ,  $\mu_{p_1|Y} := \mathbb{E}[p(\tilde{T}_1|Y)]$  and  $\mathbb{V}$  is the variance function.

The formulas of concrete form of  $G$  and  $Q$  are given in Appendix D. The proof is given in Appendix E.1.

We now analyze the gap  $\Delta_S(\tilde{T}_{IB}; \tilde{T}_1^*)$  and  $\Delta_S(\tilde{T}_s; \tilde{T}_1^*)$  by analyzing the  $\tilde{T}_1$  relevant terms. We first note that we have the following property for the IBNorm.

**Proposition 4** (Entropy Reduction). *For any random vector  $Z \in \mathbb{R}^d$  with distribution  $\mathbb{P}_Z$ , the compression operation  $s_\lambda$  in IBNorm satisfies*

$$H(s_\lambda(Z)) \leq H(Z), \quad (17)$$

where  $H(\cdot)$  denotes differential entropy. The detailed proof is given in Appendix E.3.

Based on Proposition 4, we have the following lemma.

**Lemma 5. 1)** *Let  $\tilde{T}_{IB} = s_\lambda(\tilde{T}_s)$ , where  $s_\lambda$  is a bounded-compression mapping with Lipschitz constant  $L_1 = \prod_{i=1}^d \frac{1}{\lambda}$ . For any small  $\delta > 0$ , the following holds:*

$$\mathbb{P}(\mathbb{V}(H(\tilde{T}_{IB}|X)) \leq \mathbb{V}(H(\tilde{T}_s|X))) \geq 1 - \delta, \quad \mathbb{P}(\mathbb{V}(H(\tilde{T}_{IB}|Y)) \leq \mathbb{V}(H(\tilde{T}_s|Y))) \geq 1 - \delta.$$

**2)** *In addition, let  $\tilde{T}_1, \tilde{T}'_1 \in \tilde{\mathcal{T}}_1$  be two arbitrary elements in the representation space. Then, for any  $\delta \in (0, 1)$ , the following holds with probability at least  $1 - \delta$ :*

$$\begin{aligned} |\mathbb{V}(p(\tilde{T}_1|X)) - \mathbb{V}(p(\tilde{T}'_1|X))| &\leq \delta, \\ |\mathbb{V}(p(\tilde{T}_1|Y)) - \mathbb{V}(p(\tilde{T}'_1|Y))| &\leq \delta, \\ |\mathbb{E}[p(\tilde{T}_1|X)] - \mathbb{E}[p(\tilde{T}'_1|X)]| &\leq \delta, \\ |\mathbb{E}[p(\tilde{T}_1|Y)] - \mathbb{E}[p(\tilde{T}'_1|Y)]| &\leq \delta, \end{aligned}$$

where the expectation and variance are taken with respect to the Lebesgue measure on  $\mathcal{X} \times \mathcal{Y}$ . The detailed proof is given in Appendix E.4.

Since  $G(\cdot)$  is monotone in its variance arguments, Lemma 5 implies that, given arbitrary  $\beta \in [0, 1]$  and  $\delta \in (0, 1)$ , with probability at least  $1 - \delta$  over the sample set  $S \sim \mathbb{P}(X, Y)$  with size  $M$ , the following inequality holds:

$$\Delta_S(\tilde{T}_{IB}; \tilde{T}_1^*) \leq \Delta_S(\tilde{T}_s; \tilde{T}_1^*).$$

Thus, given the hyperparameter  $\beta$  and the sample set  $S \sim \mathbb{P}(X, Y)$  with size  $M$ , we have

$$\widehat{\text{IB}}_S(T_{IB}) \geq \widehat{\text{IB}}_S(T_s) \quad \text{almost surely.}$$

□

## E.2. Proof for Lemma 3

**Lemma.** *Given a fixed trade-off hyperparameter  $\beta > 0$  and a confidence parameter  $\delta \in (0, 1)$ , the following holds with probability at least  $1 - \delta$  over the sample set  $S$ : for any representation  $\tilde{T}_1 \in \tilde{\mathcal{T}}_1$ ,*

$$\Delta_S(\tilde{T}_1; \tilde{T}_1^*) \leq G(\sigma_{H_1|X}, \sigma_{H_1|Y}, \sigma_{p_1|X}, \sigma_{p_1|Y}, \mu_{p_1|X}, \mu_{p_1|Y}) + Q(T_1^*).$$

where  $G(\cdot)$  is a monotonically increasing function with its arguments. Specifically,  $\sigma_{H_1|X} := \mathbb{V}(H(\tilde{T}_1|X))$ ,  $\sigma_{H_1|Y} := \mathbb{V}(H(\tilde{T}_1|Y))$ ,  $\sigma_{p_1|X} := \mathbb{V}(p(\tilde{T}_1|X))$ ,  $\sigma_{p_1|Y} := \mathbb{V}(p(\tilde{T}_1|Y))$ ,  $\mu_{p_1|X} := \mathbb{E}[p(\tilde{T}_1|X)]$ ,  $\mu_{p_1|Y} := \mathbb{E}[p(\tilde{T}_1|Y)]$  and  $\mathbb{V}$  is the variance function.

The formulas of concrete form of  $G$  and  $Q$  are given in Appendix D.

*Proof.* Let  $\tilde{T}_1$  be the embeddings derived from a neural network based on the sample set  $S$ .

We define the population IB value as  $\text{IB}(T) := I(Y; T) - \beta I(X; T)$  and empirical IB value as  $\widehat{\text{IB}}(T) := \widehat{I}(Y; T) - \beta \widehat{I}(X; T)$  for brevity. We denote the optimum IB representation achieving the maximum population IB value by  $\tilde{T}_1^*$ .

We define the optimum  $\tilde{T}_1^*$  of one-layer IB objective as:

$$\tilde{T}_1^* \in \arg \max_{\tilde{T}_1} (I(Y; \tilde{T}_1) - \beta I(\tilde{T}_0; \tilde{T}_1)), \quad (18)$$

where  $\tilde{T}_0 = X$ .

Given the dataset  $S \sim \mathbb{P}_{X,Y}$  with size  $M$ , we consider the empirical gap  $\Delta_S(\tilde{T}_1; \tilde{T}_1^*)$  between the IB bottleneck derived from arbitrary representation  $\tilde{T}_1$  and the optimum representation  $\tilde{T}_1^*$ , i.e.

$$\Delta_S(\tilde{T}_1; \tilde{T}_1^*) = |\widehat{I}(Y; \tilde{T}_1) - \beta \widehat{I}(X; \tilde{T}_1)| - |\widehat{I}(Y; \tilde{T}_1^*) - \beta \widehat{I}(X; \tilde{T}_1^*)|, \quad (19)$$

where  $\tilde{T}_0 = \tilde{T}_1^* = X$ . We have:

$$\Delta_S(\tilde{T}_1; \tilde{T}_1^*) = |\widehat{I}(Y; \tilde{T}_1) - \beta \widehat{I}(X; \tilde{T}_1)| - |\widehat{I}(Y; \tilde{T}_1^*) - \beta \widehat{I}(X; \tilde{T}_1^*)| \quad (20)$$

$$\leq \underbrace{|\widehat{I}(Y; \tilde{T}_1) - \widehat{I}(Y; \tilde{T}_1^*)|}_I + \underbrace{\beta |\widehat{I}(X; \tilde{T}_1) - \widehat{I}(X; \tilde{T}_1^*)|}_{II} \quad (21)$$

For any real-valued vector  $\mathbf{a} = (a_1, \dots, a_n)$ , we define the function  $V(\mathbf{a}) = \sum_{i=1}^n (a_i - \frac{1}{n} \sum_{j=1}^n a_j)^2$ . Note that  $\frac{1}{n} V(\mathbf{a})$  is simply the variance of the elements of  $\mathbf{a}$ .

In addition, we define an auxiliary real-valued function

$$\phi(x) = \begin{cases} -\frac{1}{e}, & x < -\frac{1}{e}, \\ -x \log \frac{1}{-x}, & -\frac{1}{e} < x \leq 0, \\ 0, & x = 0, \\ x \log \frac{1}{x}, & 0 < x \leq \frac{1}{e}, \\ \frac{1}{e}, & x > \frac{1}{e}. \end{cases}$$

Note that  $\phi$  is a continuous, and concave function, and that  $\lim_{x \rightarrow 0} \phi(x) = 0$ . In addition, we have the following properties for the auxiliary function  $\phi(\cdot)$  (Shamir et al., 2010):

**Lemma 6.** *For any  $a, b \in [0, 1]$ ,  $|a \log(a) - b \log(b)| \leq \phi(a - b)$ .*

**Lemma 7.** *For any real numbers  $a$  and  $b$ , we have  $\phi(a + b) \leq \phi(|a|) + \phi(|b|)$ .*

**I. Bound on  $|\widehat{I}(Y; \tilde{T}_1) - \widehat{I}(Y; \tilde{T}_1^*)|$ .**

Without loss of generality and reduce the complexity, we denote  $T \equiv \tilde{T}_1$  and  $T^* \equiv \tilde{T}_1^*$ . By the triangle inequality, we have:

$$|\hat{I}(Y; T) - \hat{I}(Y; T^*)| \leq \underbrace{|I(Y; T) - \hat{I}(Y; T)|}_A + \underbrace{|I(Y; T^*) - \hat{I}(Y; T^*)|}_B + \underbrace{|I(Y; T) - I(Y; T^*)|}_C.$$

To bound the terms  $A'$  and  $B'$ , we extend the results of Section 6.2 in (Shamir et al., 2010) to derive a general bound  $|I(Y; T) - \hat{I}(Y; T)|$  under the setting where  $T$  is a continuous random variable. Firstly, using the relationship  $I(Y; T) = H(T) - H(T|Y)$ , we apply the triangle inequality:

$$|I(Y; T) - \hat{I}(Y; T)| \leq |H(T) - \hat{H}(T)| + |H(T|Y) - \hat{H}(T|Y)| \quad (22)$$

### Step 1: Bounding $|H(T) - \hat{H}(T)|$

By Lemma 6, for any two densities  $p(t)$  and  $\hat{p}(t)$ , we have:

$$|H(T) - \hat{H}(T)| = \left| \int_{\mathcal{T}} p(t) \log p(t) dt - \int_{\mathcal{T}} \hat{p}(t) \log \hat{p}(t) dt \right| \leq \int_{\mathcal{T}} \phi(|p(t) - \hat{p}(t)|) dt \quad (23)$$

The difference in densities is:

$$|p(t) - \hat{p}(t)| = \left| \sum_x p(t|x)(p(x) - \hat{p}(x)) \right| \quad (24)$$

Using the Cauchy-Schwarz inequality and the definition of  $V(p(t|x))$  yields:

$$|p(t) - \hat{p}(t)| \leq \|p(x) - \hat{p}(x)\|_2 \sqrt{V(p(T = t|x))} \quad (25)$$

Substituting this back into the integral in Equation 23 gives:

$$|H(T) - \hat{H}(T)| \leq \int_{\mathcal{T}} \phi \left( \|p(x) - \hat{p}(x)\|_2 \sqrt{V(p(T = t|x))} \right) dt \quad (26)$$

### Step 2: Bounding $|H(T|Y) - \hat{H}(T|Y)|$

We decompose the difference into two terms:

$$|H(T|Y) - \hat{H}(T|Y)| \leq \left| \sum_y p(y)(H(T|y) - \hat{H}(T|y)) \right| + \left| \sum_y (p(y) - \hat{p}(y))\hat{H}(T|y) \right| \quad (27)$$

We have the following bound for the first term:

$$\left| \sum_y p(y)(H(T|y) - \hat{H}(T|y)) \right| \leq \sum_y p(y) \int_{\mathcal{T}} \phi(|p(t|y) - \hat{p}(t|y)|) dt \quad (28)$$

$$\leq \sum_y p(y) \int_{\mathcal{T}} \phi \left( \|\hat{p}(x|y) - p(x|y)\|_2 \sqrt{V(p(T = t|x))} \right) dt \quad (29)$$

By the Cauchy-Schwarz inequality, the second term can be bounded as:

$$\left| \sum_y (p(y) - \hat{p}(y))\hat{H}(T|y) \right| \leq \|p(y) - \hat{p}(y)\|_2 \sqrt{V(\hat{H}(T|Y))} \quad (30)$$

### Step 3: Final Combination

Combining the bounds for  $H(T)$  and  $H(T|Y)$  in Equations 26 and 30 and extending the results in Section 6 (Shamir et al., 2010), the following inequality holds:

---


$$|I(Y; T) - \hat{I}(Y; T)| \leq (2 + \sqrt{2 \log((|\mathcal{Y}| + 2)/\delta)}) \sqrt{\frac{V(\hat{H}(T|Y))}{M}} \quad (31)$$

$$+ 2 \int_{\mathcal{T}} \phi \left( (2 + \sqrt{2 \log((|\mathcal{Y}| + 2)/\delta)}) \sqrt{\frac{V(p(T|X))}{M}} \right) p_T(t) dt \quad (32)$$

$$\leq (2 + \sqrt{2 \log((|\mathcal{Y}| + 2)/\delta)}) \sqrt{\frac{V(H(T|Y))}{M}} \quad (33)$$

$$+ 2 \int_{\mathcal{T}} \phi \left( (2 + \sqrt{2 \log((|\mathcal{Y}| + 2)/\delta)}) \sqrt{\frac{V(p(T|X))}{M}} \right) p_T(t) dt \quad (\text{Law of Large Numbers}) \quad (34)$$

Without loss of generality, Equation 31 implies:

A)

$$\begin{aligned} |I(Y; T) - \hat{I}(Y; T)| &\leq (2 + \sqrt{2 \log((|\mathcal{Y}| + 2)/\delta)}) \sqrt{\frac{V(\hat{H}(T|Y))}{M}} \\ &+ 2 \int_{\mathcal{T}} \phi \left( (2 + \sqrt{2 \log((|\mathcal{Y}| + 2)/\delta)}) \sqrt{\frac{V(p(T|X))}{M}} \right) p_T(t) dt \\ &\leq (2 + \sqrt{2 \log((|\mathcal{Y}| + 2)/\delta)}) \sqrt{\frac{V(H(T|Y))}{M}} \\ &+ 2 \int_{\mathcal{T}} \phi \left( (2 + \sqrt{2 \log((|\mathcal{Y}| + 2)/\delta)}) \sqrt{\frac{V(p(T|X))}{M}} \right) p_T(t) dt \end{aligned}$$

B)

$$\begin{aligned} |I(Y; T^*) - \hat{I}(Y; T^*)| &\leq (2 + \sqrt{2 \log((|\mathcal{Y}| + 2)/\delta)}) \sqrt{\frac{V(\hat{H}(T^*|Y))}{M}} \\ &+ 2 \int_{\mathcal{T}^*} \phi \left( (2 + \sqrt{2 \log((|\mathcal{Y}| + 2)/\delta)}) \sqrt{\frac{V(p(T^*|X))}{M}} \right) p_{T^*}(t) dt \\ &\leq (2 + \sqrt{2 \log((|\mathcal{Y}| + 2)/\delta)}) \sqrt{\frac{V(H(T^*|Y))}{M}} \\ &+ 2 \int_{\mathcal{T}^*} \phi \left( (2 + \sqrt{2 \log((|\mathcal{Y}| + 2)/\delta)}) \sqrt{\frac{V(p(T^*|X))}{M}} \right) p_{T^*}(t) dt \end{aligned}$$

For term C, we have

C)

$$|I(Y; T) - I(Y; T^*)| \leq |H(T|Y) - H(T^*|Y)| + |H(T) - H(T^*)|$$

i)

$$\begin{aligned}
|H(T|Y) - H(T^*|Y)| &= \left| \sum_y p(y) (H(T|y) - H(T^*|y)) \right| \\
&= \left| \sum_y p(y) \int_{\mathcal{T}} p_{T|Y}(t|y) \log(p_{T|Y}(t|y)) dt - \sum_y p(y) \int_{\mathcal{T}^*} p_{T^*|Y}(t|y) \log(p_{T^*|Y}(t|y)) dt \right| \\
&\leq \sum_y p(y) \left| \int_{\mathcal{T}} p_{T|Y}(t|y) \log(p_{T|Y}(t|y)) - p_{T^*|Y}(t|y) \log(p_{T^*|Y}(t|y)) dt \right| \\
&\leq \sum_y p(y) \int_{\mathcal{T}} |p_{T|Y}(t|y) \log(p_{T|Y}(t|y)) - p_{T^*|Y}(t|y) \log(p_{T^*|Y}(t|y))| dt \\
&\leq \sum_y p(y) \int_{\mathcal{T}} \phi(p_{T|Y}(t|y) - p_{T^*|Y}(t|y)) dt \quad (\text{By Lemma 6}) \\
&= \sum_y p(y) \int_{\mathcal{T}} \phi(p_{T|Y}(t|y) - \mathbb{E}[p_{T|Y}(t|y)] + \mathbb{E}[p_{T|Y}(t|y)] - p_{T^*|Y}(t|y)) dt \\
&\leq \sum_y p(y) \int_{\mathcal{T}} \phi(|p_{T|Y}(t|y) - \mathbb{E}[p_{T|Y}(t|y)]|) + \phi(|\mathbb{E}[p_{T|Y}(t|y)]|) + \phi(|p_{T^*|Y}(t|y)|) dt \quad (\text{By Lemma 7}) \\
&\leq \sum_y p(y) \int_{\mathcal{T}} \phi(\sqrt{V(p_{T|Y}(t|y))}) + \phi(\mathbb{E}[p_{T|Y}(t|y)]) + \phi(p_{T^*|Y}(t|y)) dt
\end{aligned} \tag{35}$$

ii)

$$\begin{aligned}
|H(T) - H(T^*)| &= \left| \int_{\mathcal{T}} p_T(t) \log(p_T(t)) dt - \int_{\mathcal{T}^*} p_{T^*}(t) \log(p_{T^*}(t)) dt \right| \\
&\leq \left| \int_{\mathcal{T}} p_T(t) \log(p_T(t)) - p_{T^*}(t) \log(p_{T^*}(t)) dt \right| \\
&\leq \int_{\mathcal{T}} \sum_x p(x) |p_{T|X}(t|x) \log(p_{T|X}(t|x)) - p_{T^*|X}(t|x) \log(p_{T^*|X}(t|x))| dt \quad (\text{By Lemma 6}) \\
&\leq \int_{\mathcal{T}} \sum_x p(x) \phi(p_{T|X}(t|x) - p_{T^*|X}(t|x)) dt \\
&\leq \int_{\mathcal{T}} \sum_x p(x) [\phi(\sqrt{V(p_{T|X}(t|x))}) + \phi(\mathbb{E}[p_{T|X}(t|x)]) + \phi(p_{T^*|X}(t|x))] dt
\end{aligned} \tag{36}$$

Combining i) and ii), we yield

$$\begin{aligned}
|\hat{I}(Y; T) - \hat{I}(Y; T^*)| &\leq \sum_y p(y) \int_{\mathcal{T}} \phi(\sqrt{V(p_{T|Y}(t|y))}) + \phi(\mathbb{E}[p_{T|Y}(t|y)]) + \phi(p_{T^*|Y}(t|y)) dt \\
&\quad + \int_{\mathcal{T}} \sum_x p(x) [\phi(\sqrt{V(p_{T|X}(t|x))}) + \phi(\mathbb{E}[p_{T|X}(t|x)]) + \phi(p_{T^*|X}(t|x))] dt
\end{aligned} \tag{37}$$

Thus, in our setting, we obtain:

$$\begin{aligned}
|(\hat{I}(Y; \tilde{T}_1) - \hat{I}(Y; \tilde{T}_1^*))| &\leq (2 + \sqrt{2 \log((|\mathcal{Y}| + 2)/\delta)}) \sqrt{\frac{V(H(\tilde{T}_1|Y))}{M}} \\
&\quad + 2 \int_{\tilde{\mathcal{T}}_1} \phi \left( (2 + \sqrt{2 \log((|\mathcal{Y}| + 2)/\delta)}) \sqrt{\frac{V(p(\tilde{T}_1|X))}{M}} \right) p_{\tilde{T}_1}(t) dt \\
&\quad + (2 + \sqrt{2 \log((|\mathcal{Y}| + 2)/\delta)}) \sqrt{\frac{V(H(\tilde{T}_1^*|Y))}{M}} \\
&\quad + 2 \int_{\tilde{\mathcal{T}}_1^*} \phi \left( (2 + \sqrt{2 \log((|\mathcal{Y}| + 2)/\delta)}) \sqrt{\frac{V(p(\tilde{T}_1^*|X))}{M}} \right) p_{\tilde{T}_1^*}(t) dt \\
&\quad + \sum_y p(y) \int_{\tilde{\mathcal{T}}_1} \phi(\sqrt{V(p_{\tilde{T}_1|Y}(t|y))}) + \phi(\mathbb{E}[p_{\tilde{T}_1|Y}(t|y)]) + \phi(p_{\tilde{T}_1^*|Y}(t|y)) dt \\
&\quad + \int_{\tilde{\mathcal{T}}_1} \sum_x p(x) [\phi(\sqrt{V(p_{\tilde{T}_1|X}(t|x))}) + \phi(\mathbb{E}[p_{\tilde{T}_1|X}(t|x)]) + \phi(p_{\tilde{T}_1^*|X}(t|x))] dt
\end{aligned} \tag{38}$$

## II. Bound on $\beta |(\hat{I}(X; \tilde{T}_1) - \hat{I}(X; \tilde{T}_1^*))|$ .

Without loss of generality and reduce the complexity, we denote  $T \equiv \tilde{T}_1$  and  $T^* \equiv \tilde{T}_1^*$ . By the triangle inequality, we have:

$$|\hat{I}(X; T) - \hat{I}(X; T^*)| \leq \underbrace{|I(X; T) - \hat{I}(X; T)|}_{A'} + \underbrace{|I(X; T^*) - \hat{I}(X; T^*)|}_{B'} + \underbrace{|I(X; T) - I(X; T^*)|}_{C'}$$

To bound the terms  $A'$  and  $B'$ , we extend the results of Section 6.2 in (Shamir et al., 2010) to derive the corresponding bounds. Consequently, by applying the same bounding technique stated in I, we obtain:

A')

$$\begin{aligned}
|I(X; T) - \hat{I}(X; T)| &\leq (2 + \sqrt{2 \log((|\mathcal{Y}| + 2)/\delta)}) \sqrt{\frac{V(H(T|X))}{M}} \\
&\quad + \int_{\mathcal{T}} \phi \left( (2 + \sqrt{2 \log((|\mathcal{Y}| + 2)/\delta)}) \sqrt{\frac{V(p(T|X))}{M}} \right) p_T(t) dt,
\end{aligned} \tag{39}$$

B')

$$\begin{aligned}
|I(X; T^*) - \hat{I}(X; T^*)| &\leq (2 + \sqrt{2 \log((|\mathcal{Y}| + 2)/\delta)}) \sqrt{\frac{V(H(T^*|X))}{M}} \\
&\quad + \int_{\mathcal{T}^*} \phi \left( (2 + \sqrt{2 \log((|\mathcal{Y}| + 2)/\delta)}) \sqrt{\frac{V(p(T^*|X))}{M}} \right) p_{T^*}(t) dt.
\end{aligned} \tag{40}$$

C')

$$|I(X; T) - I(X; T^*)| \leq |H(T|X) - H(T^*|X)| + |H(T) - H(T^*)| \tag{41}$$

As shown in the C)  $|I(Y; T) - I(Y; T^*)|$  case, similarly, we have

$$\begin{aligned}
|I(X; T) - I(X; T^*)| &\leq \sum_x p(x) \int_{\mathcal{T}} \phi(\sqrt{V(p_{T|X}(t|x))}) + \phi(\mathbb{E}[p_{T|X}(t|x)]) + \phi(p_{T^*|X}(t|x)) dt \\
&\quad + \int_{\mathcal{T}} \sum_x p(x) [\phi(\sqrt{V(p_{T|X}(t|x))}) + \phi(\mathbb{E}[p_{T|X}(t|x)]) + \phi(p_{T^*|X}(t|x))] dt
\end{aligned} \tag{42}$$

Thus, in our setting, we yield

$$\begin{aligned}
\beta |\hat{I}(X; \tilde{T}_l) - \hat{I}(X; \tilde{T}_l^*)| &\leq \beta(2 + \sqrt{2 \log((|\mathcal{Y}| + 2)/\delta)}) \sqrt{\frac{V(H(\tilde{T}_l|X))}{M}} \\
&\quad + \beta \int_{\tilde{\mathcal{T}}_1} \phi \left( (2 + \sqrt{2 \log((|\mathcal{Y}| + 2)/\delta)}) \sqrt{\frac{V(p(\tilde{T}_1|X))}{M}} \right) p_{\tilde{T}_1}(t) dt \\
&\quad + \beta(2 + \sqrt{2 \log((|\mathcal{Y}| + 2)/\delta)}) \sqrt{\frac{V(H(\tilde{T}_l^*|X))}{M}} \\
&\quad + \beta \int_{\tilde{\mathcal{T}}_1^*} \phi \left( (2 + \sqrt{2 \log((|\mathcal{Y}| + 2)/\delta)}) \sqrt{\frac{V(p(\tilde{T}_1^*|X))}{M}} \right) p_{\tilde{T}_1^*}(t) dt \\
&\quad + \beta \sum_x p(x) \int_{\tilde{\mathcal{T}}_1} \phi(\sqrt{V(p_{\tilde{T}_1|X}(t|x))}) + \phi(\mathbb{E}[p_{\tilde{T}_1|X}(t|x)]) + \phi(p_{\tilde{T}_1^*|X}(t|x)) dt \\
&\quad + \int_{\tilde{\mathcal{T}}_1} \sum_x p(x) [\phi(\sqrt{V(p_{\tilde{T}_1|X}(t|x))}) + \phi(\mathbb{E}[p_{\tilde{T}_1|X}(t|x)]) + \phi(p_{\tilde{T}_1^*|X}(t|x))] dt
\end{aligned} \tag{43}$$

Combining I and II results in the following bound:

$$\begin{aligned}
\Delta_S(\tilde{T}_1; \tilde{T}_1^*) &\leq \sum_{l=1}^L \left( (2 + \sqrt{2 \log((|\mathcal{Y}| + 2)/\delta)}) \sqrt{\frac{V(H(\tilde{T}_l|Y))}{M}} \right. \\
&\quad + 2 \int_{\tilde{\mathcal{T}}_1} \phi \left( (2 + \sqrt{2 \log((|\mathcal{Y}| + 2)/\delta)}) \sqrt{\frac{V(p(\tilde{T}_1|X))}{M}} \right) p_{\tilde{T}_1}(t) dt \\
&\quad + (2 + \sqrt{2 \log((|\mathcal{Y}| + 2)/\delta)}) \sqrt{\frac{V(H(\tilde{T}_1^*|Y))}{M}} \\
&\quad + 2 \int_{\tilde{\mathcal{T}}_1^*} \phi \left( (2 + \sqrt{2 \log((|\mathcal{Y}| + 2)/\delta)}) \sqrt{\frac{V(p(\tilde{T}_1^*|X))}{M}} \right) p_{\tilde{T}_1^*}(t) dt \\
&\quad + \sum_y p(y) \int_{\tilde{\mathcal{T}}_1} \phi(\sqrt{V(p_{\tilde{T}_1|Y}(t|y))}) + \phi(\mathbb{E}[p_{\tilde{T}_1|Y}(t|y)]) + \phi(p_{\tilde{T}_1^*|Y}(t|y)) dt \\
&\quad \left. + \beta(2 + \sqrt{2 \log((|\mathcal{Y}| + 2)/\delta)}) \sqrt{\frac{V(H(\tilde{T}_1|X))}{M}} \right. \\
&\quad + \beta \int_{\tilde{\mathcal{T}}_1} \phi \left( (2 + \sqrt{2 \log((|\mathcal{Y}| + 2)/\delta)}) \sqrt{\frac{V(p(\tilde{T}_1|X))}{M}} \right) p_{\tilde{T}_1}(t) dt \\
&\quad + \beta(2 + \sqrt{2 \log((|\mathcal{Y}| + 2)/\delta)}) \sqrt{\frac{V(H(\tilde{T}_1^*|X))}{M}} \\
&\quad + \beta \int_{\tilde{\mathcal{T}}_1^*} \phi \left( (2 + \sqrt{2 \log((|\mathcal{Y}| + 2)/\delta)}) \sqrt{\frac{V(p(\tilde{T}_1^*|X))}{M}} \right) p_{\tilde{T}_1^*}(t) dt \\
&\quad + \beta \sum_x p(x) \int_{\tilde{\mathcal{T}}_1} \phi(\sqrt{V(p_{\tilde{T}_1|X}(t|x))}) + \phi(\mathbb{E}[p_{\tilde{T}_1|X}(t|x)]) + \phi(p_{\tilde{T}_1^*|X}(t|x)) dt \\
&\quad \left. + (\beta + 1) \int_{\tilde{\mathcal{T}}_1} \sum_x p(x) [\phi(\sqrt{V(p_{\tilde{T}_1|X}(t|x))}) + \phi(\mathbb{E}[p_{\tilde{T}_1|X}(t|x)]) + \phi(p_{\tilde{T}_1^*|X}(t|x))] dt \right)
\end{aligned} \tag{44}$$

We begin by defining the main functional related to representation  $\tilde{T}_1$  that controls the generalization gap:

$$\begin{aligned}
& G(\sigma_{H_1|X}, \sigma_{H_1|Y}, \sigma_{p_1|X}, \sigma_{p_1|Y}, \mu_{p_1|X}, \mu_{p_1|Y}) \\
&= C_1 \sqrt{\frac{\sigma_{H_1|X}}{M}} + C_1 \sqrt{\frac{\sigma_{H_1|Y}}{M}} + \sum_y p(y) \int_{\tilde{\mathcal{T}}_1} \phi(\sqrt{\sigma_{p_1|Y}}) dt + \beta \sum_x p(x) \int_{\tilde{\mathcal{T}}_1} \phi(\sqrt{\sigma_{p_1|X}}) dt \\
&+ (\beta + 2) \int_{\tilde{\mathcal{T}}_1} \phi\left(C_1 \sqrt{\frac{\sigma_{H_1|X}}{M}}\right) p_{\tilde{T}_1}(t) dt + \sum_y p(y) \int_{\tilde{\mathcal{T}}_1} \phi(\mu_{p_1|Y}) dt + \beta \sum_x p(x) \int_{\tilde{\mathcal{T}}_1} \phi(\mu_{p_1|X}) dt \\
&+ (\beta + 1) \int_{\tilde{\mathcal{T}}_1} \sum_x p(x) [\phi(\sqrt{\sigma_{p_1|X}}) + \phi(\mu_{p_1|X})] dt,
\end{aligned} \tag{45}$$

where

$$\begin{aligned}
\sigma_{H_1|X} &:= V(H(\tilde{T}_1|X)) = |\mathcal{X}|\mathbb{V}(H(\tilde{T}_1|X)), & \sigma_{H_1|Y} &:= V(H(\tilde{T}_1|Y)) = |\mathcal{Y}|\mathbb{V}(H(\tilde{T}_1|Y)), \\
\sigma_{p_1|X} &:= V(p(\tilde{T}_1|X)) = |\mathcal{X}|\mathbb{V}(p(\tilde{T}_1|X)), & \sigma_{p_1|Y} &:= V(p(\tilde{T}_1|Y)) = |\mathcal{Y}|\mathbb{V}(p(\tilde{T}_1|Y)), \\
\mu_{p_1|X} &:= \mathbb{E}[p(\tilde{T}_1|X)], & \mu_{p_1|Y} &:= \mathbb{E}[p(\tilde{T}_1|Y)],
\end{aligned}$$

and

$$C_1 = 2 + \sqrt{2 \log((|\mathcal{Y}| + 2)/\delta)}.$$

$\tilde{T}_1^*$  should satisfy the self-consistent equations (Tishby et al., 2000):

$$\begin{aligned}
p(\tilde{T}_1^*|X) &= \frac{p(\tilde{T}_1^*)}{Z(\tilde{T}_0, \beta)} \exp \left[ -\beta \sum_y p(Y=y|\tilde{T}_0) \log \frac{p(Y=y|\tilde{T}_0)}{p(Y=y|\tilde{T}_1^*)} \right], \\
p(Y|\tilde{T}_1^*) &= \frac{1}{p(\tilde{T}_1^*)} \int_{\tilde{\mathcal{T}}_0} p(Y|\tilde{T}_0=t) p(\tilde{T}_1^*|\tilde{T}_0=t) p(\tilde{T}_0=t) dt, \\
p(\tilde{T}_1^*) &= \int_{\tilde{\mathcal{T}}_0} p(\tilde{T}_1^*|\tilde{T}_0=t) p(\tilde{T}_0=t) dt
\end{aligned} \tag{46}$$

where  $Z(\tilde{T}_0^*, \beta)$  is the partition function. Thus, we can write the remaining terms to optimum-dependent components:

$$\begin{aligned}
Q(\tilde{T}_1^*) &= (2 + \sqrt{2 \log((|\mathcal{Y}| + 2)/\delta)}) \sqrt{\frac{V(H(\tilde{T}_1^*|Y))}{M}} \\
&+ \beta(2 + \sqrt{2 \log((|\mathcal{Y}| + 2)/\delta)}) \sqrt{\frac{V(H(\tilde{T}_1^*|X))}{M}} \\
&+ (\beta + 2) \int_{\tilde{\mathcal{T}}_1^*} \phi\left((2 + \sqrt{2 \log((|\mathcal{Y}| + 2)/\delta)}) \sqrt{\frac{V(p(\tilde{T}_1^*|X))}{M}}\right) p_{\tilde{T}_1^*}(t) dt \\
&+ \sum_y p(y) \int_{\tilde{\mathcal{T}}_1} \phi(p_{\tilde{T}_1^*|Y}(t|y)) dt + \beta \sum_x p(x) \int_{\tilde{\mathcal{T}}_1} \phi(p_{\tilde{T}_1^*|X}(t|x)) dt + (\beta + 1) \int_{\tilde{\mathcal{T}}_1} \phi(p(\tilde{T}_1^*)) dt \\
&+ (\beta + 1) \int_{\tilde{\mathcal{T}}_1} \sum_x p(x) \phi(p_{\tilde{T}_1^*|X}(t|x)) dt \quad (\text{By Eqn. (46)})
\end{aligned} \tag{47}$$

Thus, we now can decompose the gap as the following form:

$$\Delta_S(\tilde{T}_1; \tilde{T}_1^*) \leq G(\sigma_{H_1|X}, \sigma_{H_1|Y}, \sigma_{p_1|X}, \sigma_{p_1|Y}, \mu_{p_1|X}, \mu_{p_1|Y}) + Q(\tilde{T}_1^*). \tag{48}$$

□

### E.3. Proof for Proposition 4

**Proposition** (Entropy Reduction). *For any random vector  $Z \in \mathbb{R}^d$  with distribution  $\mathbb{P}_Z$ , the compression operation  $s_\lambda$  in IBNorm satisfies*

$$H(s_\lambda(Z)) \leq H(Z),$$

where  $H(\cdot)$  denotes differential entropy.

*Proof.* Since  $s_\lambda$  is measurable and strictly monotone non-decreasing, it is an invertible mapping on its range. Let  $J_{s_\lambda}(Z)$  denote the Jacobian matrix of  $s_\lambda$ .

Using the change-of-variables formula for differential entropy:

$$H(s_\lambda(Z)) = H(Z) + \mathbb{E}[\log |\det J_{s_\lambda}(Z)|] \leq H(Z), \quad (49)$$

because the Jacobian of the compression operator can be written as

$$J_{s_\lambda}(Z) = D(Z) \left( I - \frac{1}{d} \mathbf{1} \mathbf{1}^\top \right), \quad (50)$$

where  $D(Z) = \text{diag}(f'_\lambda(|Z_1 - \mu|), \dots, f'_\lambda(|Z_d - \mu|))$ . The projection matrix  $I - \frac{1}{d} \mathbf{1} \mathbf{1}^\top$  has rank  $d - 1$  and operator norm at most 1, and  $f'_\lambda(x) \leq \alpha_\lambda \leq 1$  by the bounded compression property. Consequently,

$$|\det J_{s_\lambda}(Z)| \leq \alpha_\lambda^{d-1} \leq 1. \quad (51)$$

Hence,  $s_\lambda$  concentrates the distribution and does not increase entropy.  $\square$

#### E.4. Proof for Lemma 5

**Lemma. 1)** Let  $\tilde{T}_{IB} = s_\lambda(\tilde{T}_s)$ , where  $s_\lambda$  is a bounded-compression mapping with Lipschitz constant  $L_1 = \prod_{i=1}^d \frac{1}{\lambda}$ . For any small  $\delta > 0$ , the following holds:

$$\mathbb{P}(\mathbb{V}(H(\tilde{T}_{IB}|X)) \leq \mathbb{V}(H(\tilde{T}_s|X))) \geq 1 - \delta, \quad \mathbb{P}(\mathbb{V}(H(\tilde{T}_{IB}|Y)) \leq \mathbb{V}(H(\tilde{T}_s|Y))) \geq 1 - \delta.$$

2) In addition, let  $\tilde{T}_1, \tilde{T}'_1 \in \tilde{\mathcal{T}}_1$  be two arbitrary elements in the representation space. Then, for any  $\delta \in (0, 1)$ , the following holds with probability at least  $1 - \delta$ :

$$\begin{aligned} |\mathbb{V}(p(\tilde{T}_1|X)) - \mathbb{V}(p(\tilde{T}'_1|X))| &\leq \delta, \\ |\mathbb{V}(p(\tilde{T}_1|Y)) - \mathbb{V}(p(\tilde{T}'_1|Y))| &\leq \delta, \\ |\mathbb{E}[p(\tilde{T}_1|X)] - \mathbb{E}[p(\tilde{T}'_1|X)]| &\leq \delta, \\ |\mathbb{E}[p(\tilde{T}_1|Y)] - \mathbb{E}[p(\tilde{T}'_1|Y)]| &\leq \delta, \end{aligned}$$

where the expectation and variance are taken with respect to the Lebesgue measure on  $\mathcal{X} \times \mathcal{Y}$ .

*Proof.* 1) We first prove the first part of the Lemma.

We consider the two representations:

$$\tilde{T}_s = \Phi_s(X') = \eta \circ \psi_s \circ \zeta(X'), \quad \tilde{T}_{IB} = \Phi_{IB}(X') = \eta \circ \psi_{IB} \circ \zeta(X'),$$

where  $X' = h(X)$ ,  $\psi_{IB} = \psi_s \circ s_\lambda$  with  $s_\lambda$  being the compression operation in IBNorm.

From the Proposition 4, we have for any fixed input  $Z$ :

$$H(\psi_{IB}(Z)) = H(\psi_s(s_\lambda(Z))) \leq H(\psi_s(Z)). \quad (52)$$

Thus, the conditional entropy of  $\tilde{T}_{IB}$  is pointwise bounded by that of  $\tilde{T}_s$ .

Applying this to the conditional distributions  $\tilde{T}_{IB}|X$  and  $\tilde{T}_s|X$ , we get:

$$H(\tilde{T}_{IB}|X) \leq H(\tilde{T}_s|X), \quad H(\tilde{T}_{IB}|Y) \leq H(\tilde{T}_s|Y). \quad (53)$$

If we consider the entropy  $H$  in the discrete case, we can directly derive the relationship: consider the conditional entropy as a random variable over  $X$  (or  $Y$ ). Let  $f'(Z) := H(s_\lambda(Z))$ , then the operator norm satisfies

$$\|J_{s_\lambda}(z)\|_{\text{op}} = \max_{1 \leq i \leq d} |f'_\lambda(|z_i - \mu|)| \leq \alpha_\lambda \leq 1, \quad (54)$$

which implies that  $s_\lambda$  is  $\alpha_\lambda$ -Lipschitz, where  $\alpha_\lambda \leq 1$  by the bounded compression property of  $f_\lambda$ . Thus,  $s_\lambda$  is a Lipschitz map with Lipschitz constant  $L \leq 1$ .

Hence,  $f'(\tilde{T}_s|X)$  is a Lipschitz transformation of  $\tilde{T}_s|X$ , implying by standard variance contraction results:

$$\mathbb{V}(H(\tilde{T}_{IB}|X)) = \mathbb{V}(f'(\tilde{T}_s|X)) \leq L^2 \mathbb{V}(H(\tilde{T}_s|X)) \leq \mathbb{V}(H(\tilde{T}_s|X)).$$

Similarly,

$$\mathbb{V}(H(\tilde{T}_{IB}|Y)) \leq \mathbb{V}(H(\tilde{T}_s|Y)).$$

In the differential entropy case, we cannot guarantee a global Lipschitz constant  $L < 1$  for  $f'(\tilde{T}_s|X) = H(\tilde{T}_s|X) + \Delta'(\tilde{T}_s|X)$ . Instead, we consider a high-probability setting for the continuous random variable  $\tilde{T}_{IB}$  and  $\tilde{T}_s$ .

For any  $\delta > 0$ , let

$$\mathcal{T}_\delta^s := \{t \in \mathbb{R}^d : m_\delta \leq p_{\tilde{T}_s|X=x}(t) \leq M_\delta\}, \quad \mathbb{P}(\tilde{T}_s \in \mathcal{T}_\delta^s) \geq 1 - \delta,$$

where  $0 < m_\delta < M_\delta < \infty$ . By construction,  $\mathcal{T}_\delta^s$  is bounded:  $\exists a, b \in \mathbb{R}$ , s.t.  $\mathcal{T}_\delta^s \subset [a, b]^d$ . This ensures that the conditional density is bounded away from zero and infinity on the high-probability set.

Let  $\tilde{T}_{IB} = s_\lambda(\tilde{T}_s)$ , with  $s_\lambda$  differentiable and invertible. Then the conditional density transforms as

$$p_{\tilde{T}_{IB}|X=x}(t) = p_{\tilde{T}_s|X=x}(s_\lambda^{-1}(t)) |\det J_{s_\lambda^{-1}}(t)|, \quad (55)$$

where  $J_{s_\lambda}$  is the Jacobian of  $s_\lambda$ . The conditional differential entropy is

$$H(\tilde{T}_{IB}|X=x) = H(\tilde{T}_s|X=x) + \Delta(\tilde{T}_s), \quad \Delta(\tilde{T}_s) := \log |\det J_{s_\lambda}(\tilde{T}_s)|. \quad (56)$$

Since  $s_\lambda$  has bounded derivatives, for any  $t_1, t_2 \in \mathcal{T}_\delta^s$ ,

$$|\Delta(t_1) - \Delta(t_2)| \leq L_1 \|t_1 - t_2\|,$$

for the constant  $L_1 = \prod_{i=1}^d \alpha_\lambda = \prod_{i=1}^d \frac{1}{\lambda}$  determined by the bounds of the Jacobian of  $s_\lambda$ .

For any two conditional densities  $p_1, p_2$  of  $\tilde{T}_s|X$  supported in  $\mathcal{T}_\delta^s$ , standard results for differential entropy bounded away from zero and infinity imply

$$|H(p_1) - H(p_2)| \leq L_2 \|p_1 - p_2\|_1,$$

with  $L_2 := |\log m_\delta| + 1/m_\delta$ . Hence  $H(\tilde{T}_s|X)$  is Lipschitz on  $\mathcal{T}_\delta^s$ .

For  $\tilde{T}_s \in \mathcal{T}_\delta^s$ , we have

$$\mathbb{V}(H(\tilde{T}_{IB}|X) \mid \tilde{T}_s \in \mathcal{T}_\delta^s) = \mathbb{V}(H(\tilde{T}_s|X) + \Delta(\tilde{T}_s) \mid \tilde{T}_s \in \mathcal{T}_\delta^s). \quad (57)$$

Expanding Equation 57 using the variance formula gives

$$\mathbb{V}(H(\tilde{T}_s|X) + \Delta(\tilde{T}_s)) = \mathbb{V}(H(\tilde{T}_s|X)) + \mathbb{V}(\Delta(\tilde{T}_s)) + 2\text{Cov}(H(\tilde{T}_s|X), \Delta(\tilde{T}_s)). \quad (58)$$

Since  $\Delta(\tilde{T}_s)$  is Lipschitz with constant  $L_1$  on the bounded set  $\mathcal{T}_\delta^s \subset [a, b]^d$ , we have

$$\mathbb{V}(\Delta(\tilde{T}_s) \mid \tilde{T}_s \in \mathcal{T}_\delta^s) \leq \frac{1}{4} L_1^2 (b-a)^2. \quad (59)$$

Moreover, under the bounded-compression property of  $s_\lambda$ , the covariance term is non-positive:

$$\text{Cov}(H(\tilde{T}_s|X), \Delta(\tilde{T}_s) \mid \tilde{T}_s \in \mathcal{T}_\delta^s) \leq 0. \quad (60)$$

Combining Equations 59 and 59, we obtain:

$$\mathbb{V}(H(\tilde{T}_{IB}|X) \mid \tilde{T}_s \in \mathcal{T}_\delta^s) \leq \mathbb{V}(H(\tilde{T}_s|X) \mid \tilde{T}_s \in \mathcal{T}_\delta^s) + \frac{1}{4} L_1^2 (b-a)^2. \quad (61)$$

Similarly, for  $Y$ ,

$$\mathbb{V}(H(\tilde{T}_{IB}|Y) \mid \tilde{T}_s \in \mathcal{T}_\delta^s) \leq \mathbb{V}(H(\tilde{T}_s|Y) \mid \tilde{T}_s \in \mathcal{T}_\delta^s) + \frac{1}{4} L_1^2 (b-a)^2, \quad (62)$$

where  $L_1 = \prod_{i=1}^d \frac{1}{\lambda}$ .

---

**Remark.** The covariance term  $\text{Cov}(H(\tilde{T}_s|X), \Delta(\tilde{T}_s))$  is typically negative because, under the bounded-compression property of  $s_\lambda$ , larger conditional entropy  $H(\tilde{T}_s|X)$  corresponds to a more spread-out distribution, which is locally contracted more by  $s_\lambda$ , resulting in smaller  $\Delta(\tilde{T}_s) = \log |\det J_{s_\lambda}(\tilde{T}_s)|$ . On the high-probability set  $\mathcal{T}_\delta^s$ , any residual covariance can be made arbitrarily small by choosing  $\delta$  sufficiently small.

Based on the bounded compression property and the property of  $\Delta(\tilde{T}_s)$ , we have  $\frac{1}{4}L_1^2(b-a)^2 + 2\text{Cov}(H(\tilde{T}_s|X), \Delta(\tilde{T}_s)) \mid \tilde{T}_s \in \mathcal{T}_\delta^s \leq 0$ . Thus, we obtain

$$\mathbb{V}(H(\tilde{T}_{IB}|X) \mid \tilde{T}_s \in \mathcal{T}_\delta^s) \leq \mathbb{V}(H(\tilde{T}_s|X) \mid \tilde{T}_s \in \mathcal{T}_\delta^s), \quad (63)$$

and

$$\mathbb{V}(H(\tilde{T}_{IB}|Y) \mid \tilde{T}_s \in \mathcal{T}_\delta^s) \leq \mathbb{V}(H(\tilde{T}_s|Y) \mid \tilde{T}_s \in \mathcal{T}_\delta^s). \quad (64)$$

Finally, taking into account that  $\mathbb{P}(\tilde{T}_s \in \mathcal{T}_\delta^s) \geq 1 - \delta$  and letting  $\delta \rightarrow 0$ , we have that, for any small  $\delta > 0$ , the following holds:

$$\mathbb{P}(\mathbb{V}(H(\tilde{T}_{IB}|X)) \leq \mathbb{V}(H(\tilde{T}_s|X))) \geq 1 - \delta, \quad \mathbb{P}(\mathbb{V}(H(\tilde{T}_{IB}|Y)) \leq \mathbb{V}(H(\tilde{T}_s|Y))) \geq 1 - \delta. \quad (65)$$

2) We then prove the second part of the Lemma.

We have the following properties for the probability function  $p(\cdot)$  and variance function  $\mathbb{V}(\cdot)$  (Ash & Doléans-Dade, 2000):

**Lemma 8.** *Given the compact representation space  $\tilde{\mathcal{T}}_1$ , for any  $\delta > 0$ , there exists  $\epsilon > 0$  such that*

$$\|\tilde{T}_1 - \tilde{T}'_1\| < \epsilon \implies |p(\tilde{T}_1|X) - p(\tilde{T}'_1|X)| < \delta/2, \quad |p(\tilde{T}_1|Y) - p(\tilde{T}'_1|Y)| < \delta/2.$$

**Lemma 9.** *For any bounded functions  $f, g : \mathcal{X} \rightarrow \mathbb{R}$ ,*

$$|\mathbb{E}[f] - \mathbb{E}[g]| \leq \|f - g\|_\infty, \quad |\mathbb{V}(f) - \mathbb{V}(g)| \leq \|f - g\|_\infty \left( 2\sqrt{\mathbb{V}(f)} + \|f - g\|_\infty \right).$$

By Lemma 8, for any  $\delta > 0$ , there exists  $\epsilon > 0$  such that if  $\|\tilde{T}_1 - \tilde{T}'_1\| < \epsilon$ :

$$|p(\tilde{T}_1|X) - p(\tilde{T}'_1|X)| < \delta/2, \quad |p(\tilde{T}_1|Y) - p(\tilde{T}'_1|Y)| < \delta/2.$$

By Lemma 9, this implies

$$|\mathbb{E}[p(\tilde{T}_1|X)] - \mathbb{E}[p(\tilde{T}'_1|X)]| \leq \delta, \quad |\mathbb{E}[p(\tilde{T}_1|Y)] - \mathbb{E}[p(\tilde{T}'_1|Y)]| \leq \delta, \quad (66)$$

$$|\mathbb{V}(p(\tilde{T}_1|X)) - \mathbb{V}(p(\tilde{T}'_1|X))| \leq \delta, \quad |\mathbb{V}(p(\tilde{T}_1|Y)) - \mathbb{V}(p(\tilde{T}'_1|Y))| \leq \delta. \quad (67)$$

Since  $\tilde{T}_1, \tilde{T}'_1$  are independently drawn from a measure with full support on the compact set  $\tilde{\mathcal{T}}_1$ ,  $\|\tilde{T}_1 - \tilde{T}'_1\| < \epsilon$  holds with probability at least  $1 - \delta$ .  $\square$

## E.5. Proof for Corollary 2

**Corollary.** *With probability at least  $1 - \delta$  over training set  $S$  of size  $M < \infty$ , the generalization error of a  $L$ -layer network  $f_o$  satisfies*

$$\text{gen}(S; f_o) \leq U_o := \sum_{l=1}^L U_l^o, \quad \text{with } U_l^o = \sqrt{\frac{-IB(T_l^o) + C_S + \log(\frac{2}{\delta})}{M}},$$

where  $T_l^o$  is the intermediate representation at layer  $l$ , and  $C_S$  is a term depending on the cardinality of the training set  $S$ . Here  $f_o$  can be the network  $f_S$  using standard normalization like LN and BN, or the network  $f_{IB}$  with IBNorm.

*Proof.* Because  $\eta$  is linear and invertible, it does not affect the mutual information terms (Hjelm et al., 2018; Ash & Doléans-Dade, 2000); therefore, it suffices to analyze the intermediate representations before normalization representation recovery  $\eta$ :  $\tilde{T}_l^o := \psi_l^o \circ \zeta_l^o \circ h_l^o(X)$ ,  $l = 1, \dots, L$ . Extending the results of Appendix F.4 in (Kawaguchi et al., 2023),

we have: for arbitrary any  $\delta > 0$ , with probability at least  $1 - \delta$  over the training set  $S$  of size  $M < \infty$ , the following generalization bound holds:

$$\text{gen}(S; f_o) \leq \sum_{l=1}^L U_l^o := \sum_{l=1}^L \sqrt{\frac{I(X; \tilde{T}_l^o | Y) + C(S, f_l^o) + \log(\frac{2}{\delta})}{M}}, \quad (68)$$

where  $\tilde{T}_l$  is the intermediate representation at layer  $l$  before normalization representation recovery  $\eta$  and  $C(S, f_l^o) \propto \ln(2|\Phi_l^o||\mathcal{Y}|/\delta)$  is a term depending on the cardinality of the hypothesis space associated with the  $l$ -th layer  $f_l^o$  and the training set  $S$ . Since  $f_l^{\text{IB}}$  and  $f_l^S$  have the same parameter size, the model-complexity terms satisfy  $C(S, f_l^{\text{IB}}) \equiv C(S, f_l^S)$  for all  $l$ . Thus, for the L-layer network, we denote  $C_S := C(S, f_l^{\text{IB}}) \equiv C(S, f_l^S)$ . Thus, we obtain a bound on the total generalization error:

$$\text{gen}(S; f_o) \leq U_o := \sum_{l=1}^L U_l^o, \quad \text{with } U_l^o = \sqrt{\frac{I(X; \tilde{T}_l^o | Y) + C_S + \log(\frac{2}{\delta})}{M}}. \quad (69)$$

Given the assumption that  $\beta = 1$ , we have

$$I(X; \tilde{T}_l^o | Y) = I(X; \tilde{T}_l^o) - I(Y; \tilde{T}_l^o) = -\text{IB}(\tilde{T}_l^o). \quad (70)$$

Thus, we yield

$$\text{gen}(S; f_o) \leq U_o := \sum_{l=1}^L U_l^o, \quad \text{with } U_l^o = \sqrt{\frac{-\text{IB}(\tilde{T}_l^o) + C_S + \log(\frac{2}{\delta})}{M}}. \quad (71)$$

This establishes a layer-wise mutual information bound on the generalization error shown in Corollary 2.  $\square$

**Remark.** In our experiments, all models are trained on the same dataset  $S$ , so any dataset-dependent contribution to the generalization bound can be treated as invariant across different normalization schemes. The normalization layers considered in our study (LN, BN, and IBNorm) have identical total parameter size. Thus, the hypothesis spaces  $\Phi_l^{\text{IB}}$  and  $\Phi_l^S$  associated with  $f_l^{\text{IB}}$  and  $f_l^S$  have the same cardinality across all layers  $l$ . Theoretically, by Lemma 6 in (Kawaguchi et al., 2023), for the L-layer network, we have  $C_S := C(S, f_l^{\text{IB}}) \equiv C(S, f_l^S)$ , that is, the model-complexity terms are equivalent for  $f_l^{\text{IB}}$  and  $f_l^S$ . The generalization bound of  $f_{\text{IB}}$  and  $f_S$  therefore differ only in the representation-complexity term  $-\text{IB}(T_l^o) \equiv I(X; \tilde{T}_l^o | Y)$  across all layers  $l$ .

## F. Experimental Details

### F.1. LLM Experiments

For all LLaMA models, we follow the setup in (Zhao et al., 2024) and pretrain the vanilla LLaMA series models from scratch on the C4 dataset. We set the maximum input sequence length to 512 and output sequence length to 256, and adopt the bfloat16 precision. For the LLaMA-60M model, we use a learning rate of 0.001, mini-batch size of 64 with gradient accumulation to a global batch size of 512, 20,000 training steps with 1,000 warm-up steps, and the AdamW (Kinga et al., 2015; Loshchilov & Hutter, 2017) optimizer with  $(\beta_1, \beta_2) = (0.9, 0.999)$ . For the LLaMA-130M model, we use the same learning rate but reduce the mini-batch size to 32 with gradient accumulation to a global batch size of 512, train for 20,000 steps with 2,000 warm-up steps, and maintain the same optimizer configuration. For the LLaMA-350M model, we set the mini-batch size to 16 with gradient accumulation to a global batch size of 512, extend training to 60,000 steps with 6,000 warm-up steps. For the LLaMA-1B model, we set the mini-batch size to 16 with gradient accumulation to a global batch size of 512, extend training to 100,000 steps with 10,000 warm-up steps.

For the GPT-2 series, we follow the Sophia setup (Liu et al., 2023) with the nanoGPT implementation (Karpathy, 2022) and pretrain the vanilla GPT-2 series on OpenWebText (Gokaslan & Cohen, 2019). We set the maximum input sequence length to 1024 and adopt the bfloat16 precision. We use a global batch size of 480, cosine learning rate decay with 2,000 warm-up iterations, and global gradient clipping with a threshold of 1.0. All models are trained for 100,000 steps. We employ the AdamW optimizer with  $(\beta_1, \beta_2) = (0.9, 0.95)$  and weight decay of 0.1. For GPT-2 Small (124M), We use a per-device mini-batch size of 12 and 10 gradient accumulation steps across 4 GPUs, resulting in an effective global batch size of 480. We employ a cosine learning rate scheduler with a peak learning rate of 0.0006 and a minimum learning rate of 0.00003. For GPT-2 Medium (355M), we use a per-device mini-batch size of 10 and 12 gradient accumulation steps across 4 GPUs, resulting in an effective global batch size of 480. We employ a cosine learning rate scheduler with a peak learning rate of 0.0003 and a minimum learning rate of 0.00006.

---

For the hyperparameter noise factor in NormalNorm, we perform a lightweight Sobol-based search on the interval  $[0, 1]$ , and set the value to 1 for all experiments. For the hyperparameter  $\lambda$  in each variant of IBNorm, we conduct a grid search over the set  $\{2, 3, 4, 5\}$ . The final configurations are  $\lambda = 3$  for IBNorm-S, and  $\lambda = 4$  for both IBNorm-L and IBNorm-T. We investigated several hyperparameter configurations, including learning rate, learning rate scheduler, weight decay, and minibatch size, across all models and found the present configurations to generally work best. The statistical significance results are evaluated across three independent runs.

All models are trained on 4xNVIDIA L40-S. The total GPU training hours are about 10500 hours for all of our LLM pretraining tasks.

## F.2. Vision Experiments

**ResNet Experiments.** In all experiments involving ResNet18 on CIFAR-10, we use stochastic gradient descent (SGD) with learning rate 0.1, weight decay 0.0005, momentum 0.9, and batch size 128 for LayerNorm and NormalNorm, with a noise factor of 0.4. For IterNorm experiments, we use weight decay 0.005. For IBNorm experiments, we use weight decay 0.001. Following (Eftekhari & Papyan, 2025), models were trained from random initialization for 200 epochs, with a StepLR scheduler reducing the learning rate by a factor of 10 every 60 epochs.

For experiments with ResNet-50 on ImageNet, a batch size of 256 was used, with SGD parameters: learning rate 0.1, momentum 0.9, Nesterov acceleration enabled, and weight decay 0.0001, along with a cosine annealing learning rate scheduler with maximum 200 epochs and minimum learning rate 0.000001 for BatchNorm and NormalNorm, with a noise factor of 1. For IBNorm experiments, we use weight decay 0.001. For the hyperparameter  $\lambda$  in each variant of IBNorm, we conduct a grid search over the set  $\{2, 3, 4, 5\}$ . The final configurations are  $\lambda = 3$  for IBNorm-S, and  $\lambda = 4$  for both IBNorm-L and IBNorm-T. We explored several hyperparameter configurations, including learning rate, learning rate scheduler, weight decay, and minibatch size, across all models and found the present configurations to generally work best.

**ViT Experiments.** We train ViT-S/16 and ViT-B/16 (Dosovitskiy et al., 2020) following the setup (Yuan et al., 2021) on ImageNet. All models are trained for 300 epochs with a global batch size of 512. For ViT-S/16, we use the AdamW optimizer with a learning rate of 0.001, weight decay of 0.03, and  $(\beta_1, \beta_2) = (0.9, 0.999)$ . For ViT-B/16, the AdamW optimizer is used with a learning rate of 0.001, weight decay of 0.05, and  $(\beta_1, \beta_2) = (0.9, 0.999)$ . We adopt a hybrid learning rate schedule that combines linear warmup with cosine annealing over the first 10 training epochs. During warmup, the learning rate increases linearly from 0.000001 to the base learning rate. After warmup, cosine annealing is applied for the remaining epochs, gradually decaying the learning rate to a minimum of 0.000001.

We also follow the setup in NormalNorm (Eftekhari & Papyan, 2025) to train a ViT model with 8 transformer layers, 8 attention heads, hidden dimension size 768, MLP dimension size 2304, and patch size 16. Models were trained on ImageNet for 200 epochs with a global batch size of 512. Weighted random sampling based on inverse class frequency was applied during training to improve performance across all model configurations. The AdamW optimizer was used with learning rate 0.001, weight decay 0.05,  $(\beta_1, \beta_2) = (0.9, 0.999)$ , and epsilon 0.00000001 with a noise factor of 1. In addition, we employ a hybrid scheduling strategy that combines linear warmup with cosine annealing over 5 warmup training epochs. During the warmup phase, the learning rate increases linearly from 0.1 to 1.0 of the base learning rate. After warmup, a cosine annealing schedule is applied for the remaining epochs, with the learning rate decaying towards a minimum value of 0.000001.

For the hyperparameter  $\lambda$  in each variant of IBNorm, we conduct a grid search over the set  $\{2, 3, 4, 5\}$ . The final configurations are  $\lambda = 3$  for IBNorm-S, and  $\lambda = 4$  for both IBNorm-L and IBNorm-T. Hyperparameter configurations, including learning rate, scheduler, weight decay, and minibatch size, were explored, and the configurations reported here were found to work best across all ViT models.

All models were trained on 4xNVIDIA L40-S, RTX 3090, and Tesla V100, with a total of approximately 6500 GPU hours for all vision tasks.

## G. Mathematical Details for Matrix-Based Information Estimation

Following the approach in (Chang et al., 2025), we employ matrix-based Rényi entropy (Giraldo et al., 2014) to estimate mutual information (MI) between model representations and target labels. This method captures sample similarity structures via kernel Gram matrices.

## G.1. Matrix-Based Entropy Estimation

Let  $U = \{u_i\}_{i=1}^N$  denote  $l_2$ -normalized representations obtained after the normalization layer. A Gaussian kernel Gram matrix  $G_U \in \mathbb{R}^{N \times N}$  is constructed as:

$$(G_U)_{i,j} = \exp\left(-\frac{\|u_i - u_j\|^2}{2\sigma^2}\right),$$

with bandwidth  $\sigma = 1$ . The matrix is then trace-normalized to ensure  $\text{tr}(G_U) = 1$ .

The matrix-based Rényi entropy of order  $\alpha = 1$  is defined as:

$$H(U) = -\text{tr}(G_U \log G_U).$$

This expression can be interpreted in terms of the eigenvalue spectrum  $\{\lambda_k\}_{k=1}^N$  of  $G_U$ , since  $G_U$  is positive semi-definite and trace-normalized:

$$H(U) = -\sum_{k=1}^N \lambda_k \log \lambda_k.$$

Intuitively, a more uniform eigenvalue spectrum corresponds to higher entropy (more diverse representations), while a sharply peaked spectrum indicates redundancy or compression.

## G.2. Mutual Information Estimation

To estimate the mutual information between two random variables  $U$  and  $V$ , we compute their Gram matrices  $G_U$  and  $G_V$ , and form the joint similarity matrix via element-wise (Hadamard) product:

$$G_{UV} = G_U \circ G_V.$$

After trace-normalization, mutual information is estimated by:

$$I(U; V) = H(U) + H(V) - H(U, V).$$

where  $H(U, V) = -\text{tr}(G_{UV} \log G_{UV})$ . A more concentrated eigenvalue spectrum of  $G_{UV}$  relative to  $G_U$  and  $G_V$  indicates stronger dependence between  $U$  and  $V$ , and thus higher mutual information.

Here we demonstrate our algorithm for calculating the token-level IB value. We consider a transformer model  $f$  with  $L$  layers. Given an input sequence  $x_{1:T}$  of length  $T$ ,  $t_i^{(l)} \in \mathbb{R}^d$  denotes the hidden activation at the last token position of the  $i$ -th input sequence after  $l$ -th normalization layer, for  $l \in [L]$ . For next-token prediction, the ground-truth label is denoted by  $y_i \in \mathbb{R}^d$ , corresponding to the embedding of the true next token from the vocabulary  $\mathcal{V}$ . At a generation time step  $p$  and cross a batch of  $N$  sequences, we collect the representations:

$$T_{l-1} = \{t_i^{(l-1)}\}_{i=1}^N, T_l = \{t_i^{(l)}\}_{i=1}^N, Y = \{y_i\}_{i=1}^N,$$

where  $T_0^{(l)}$  is consisted of the batch of last input tokens  $x_T$  hidden representations. We iteratively derive those embeddings: In the first forward pass, a batch of  $N$  input sequences  $x_{1:T}$  is fed into the transformer to obtain hidden states at each layer. From these, we extract the final-token representations  $T_l, l \in [L]$ . In the second forward pass, each input is concatenated with its ground-truth next token  $y$ , and we extract the corresponding label embedding  $Y$  from the output of the embedding layer (Chang et al., 2025). Based on these sets, we can compute two information-theoretic quantities:  $I_p(Y, T_l)$  and  $I_p(T_l - 1, T_l)$  at generation timestep  $t$  across  $l \in [L]$  and aim to derive the total IB value in the network  $f$  given in Eqn. (5), as  $\mathbb{E}_p[I_p(Y, T_l)] = \hat{I}(Y, T_l)$  and  $\mathbb{E}_p[I_p(T_l - 1, T_l)] = \hat{I}(T_l - 1, T_l)$  by the Monte Carlo approximation.

In practice, we set the batch size to  $N = 64$  and iteratively compute the mutual information values during autoregressive generation until all instances reach the end-of-sequence ( $<EOS>$ ) token. During autoregressive generation in LLM tasks, different instances in a batch may terminate at different time steps upon reaching the  $<EOS>$  token. To handle this, we use a diagonal mask matrix:

$$M \in \{0, 1\}^{N \times N}, \quad M_{ii} = \begin{cases} 1, & \text{if instance } i \text{ is still active (not } <EOS> \text{)} \\ 0, & \text{if instance } i \text{ has reached } <EOS> \end{cases}.$$

For example, at each step of the generation, the masked Gram matrix for the latent embedding  $T_l$  is computed as  $\tilde{G}_{T_l} = MG_{T_l}M$  and then conducted trace-normalization.

---

### G.3. Token-Level IB Value Estimation

We apply the matrix-based framework to estimate mutual information for token-level IB analysis. Specifically, we uniformly sample  $P = 30$  timesteps across the generation process. For each sampled timestep and each layer  $l \in [L]$ , we extract the representations  $T_l$  and compute the following information-theoretic quantities:  $I_p(Y, T_l)$  and  $I_p(T_{l-1}, T_l)$  across  $l \in [L]$  at sampled timestep  $t$ . Then we sum the IB value across  $l$  and derive  $\sum_{p=1}^P \sum_{l=1}^L \left( I_p(Y; T_l) - \beta I_p(T_{l-1}; T_l) \right)$  (we always set  $\beta = 1$ ). Finally, the token-level IB value is obtained by averaging over the batch size  $N$  and the number of sampled timesteps  $P$ .